# NATIONAL ADVISORY COMMITTEE FOR AERONAUTICS

TECHNICAL NOTE

No. 1744

## TWO-DIMENSIONAL COMPRESSIBLE FLOW IN CONICAL MIXED-FLOW COMPRESSORS

By John D. Stanitz

Lewis Flight Propulsion Laboratory
Cleveland, Ohio

Washington
November 1948

NATIONAL ADVISORY COMMITTEE FOR AERONAUTICS

TECHNICAL NOTE No. 1744

# TWO-DIMENSIONAL COMPRESSIBLE FLOW IN CONICAL MIXED-FLOW COMPRESSORS

By John D. Stanitz

## SUMMARY

A general method of analysis is developed for the two-dimensional, steady, compressible flow through mixed-flow compressors in which the center line of the passage generates a right circular cone about the axis of the compressor. The two-dimensional, radial-discharge compressor is a special case in which the cone angle is equal to 180°. The variables taken into account are: (1) impeller tip Mach number, (2) compressor flow rate, (3) blade shape (curvature), (4) passage height, (5) number of blades, and (6) compressor cone angle. Relaxation methods are used to solve the resulting nonlinear differential equation for the stream function. Special attention is paid to logarithmic-spiral blades, of which the straight blade (lying on a conic radius) is a particular case.

As a result of the analysis, it is concluded that the solution obtained for a given cone angle also applies to certain other cone angles (that is, other mixed-flow compressors) with a fewer or a greater number of passages but with the same included passage angle, and so forth. It is also concluded that mixed-flow compressors with the same number of flow passages as radial-discharge compressors and therefore with smaller included passage angles have lower peak blade loadings and lower maximum relative velocities than the corresponding radial-discharge compressors.

The general analysis also applies to inward-flow turbines. In fact, the solution obtained for a centrifugal compressor with smooth (shockless) entry is also the solution (with the flow direction and rotation reversed) for an inward-flow turbine with the same design characteristics (that is, the same rotor) and with shockless entry.

A numerical example is presented consisting of a radial-discharge compressor (cone angle equal to 180°) with constant flow area and 20 straight, radial blades operating at a tip Mach number of 1.5. The results of this example are given by plots of the streamlines, lines of constant pressure ratio, and lines of constant Mach number. For the conditions of this example, a wheel-type eddy forms on the driving face of the blade; the velocities and pressures at the impeller tip are reasonably uniform; any nonuniformity in the flow leaving the impeller tip adjusts itself rapidly; the maximum local Mach number is 0.64 and occurs along the trailing face of the blade at 68 percent of the tip radius; and the computed value of the slip factor is 0.90.

In addition, a simplified analysis for straight blades lying on conic radii is presented that can be used to determine the streamlines, the pressure distribution, and the velocity profiles within the impeller except near the tip (and inlet).

## INTRODUCTION

Increased knowledge of flow conditions within centrifugal compressors can result in improved compressor performance. For example, boundary-layer growth and flow separation, which affect the compressor efficiency, can be controlled by suitable changes in the compressor design provided the effects of these changes on velocity and pressure gradients within the compressor are known.

For a given set of operating conditions, the flow conditions within centrifugal compressors depend upon the geometry of the compressor (three-dimensional effects) and upon the properties of the fluid (compressibility and viscosity). Most treatments of the problem up to the present time have been concerned with the two-dimensional-flow effects for incompressible, nonviscous fluids (for example, references 1 to 5).

In the analysis reported herein, compressibility is considered, which is especially important in centrifugal compressors because the large pressure ratios per stage result in density changes that affect the fluid velocities and therefore the streamlines, the pressure gradients, and so forth. In addition, compressibility is important in regions of supersonic flow where shock phenomena may develop. A method is developed for determining the two-dimensional, compressible, nonviscous, steady flow through mixed-flow compressors in which the center line of the passage generates a right circular

cone. The two-dimensional flow pattern is considered to lie upon the surface of this cone. The radial-discharge compressor is a special case in which the cone angle is 180°.



The solution of two-dimensional, compressible-flow equations is accomplished by a numerical procedure known as the relaxation method. This method was first developed by Southwell (references 6 and 7) and has been extended to compressible-flow problems by Emmons (reference 8). It is essentially the procedures outlined by Emmons that are employed in the numerical solution of the differential equation obtained in this analysis.

The analysis is first developed for arbitrary blade shapes and is later applied to logarithmic blade shapes of which the straight blade lying on a conic radius is a special case. A numerical example is presented with constant flow area and 20 straight blades operating at a tip Mach number of 1.5. Finally, a simplified analysis for straight blades lying on conic radii is developed that checks the results of the relaxation solution except for regions of flow near the impeller tip (and inlet).

## ANALYSIS

### General Case

This analysis develops a method whereby the streamlines, the velocity profiles, and the pressure distributions can be determined for steady, two-dimensional, compressible flow in centrifugal compressors with arbitrary blade shapes, varying flow areas, and fixed cone angles. The analysis is limited to mixed-flow compressors in which the center line of the passage generates a right circular cone with a cone angle $\alpha$ (fig. 1). (All symbols are defined in appendix A.) The two-dimensional flow pattern is considered to lie upon the surface of this cone. A developed view of the conic surface is shown in figure 2. For the special case in which $\alpha$ is 180°, the cone surface becomes plane and is normal to the axis of rotation. Such compressors ($\alpha$ = 180°) shall be designated radial-discharge centrifugal compressors. For the special case in which $\alpha$ is 0°, the cone surface becomes cylindrical and is concentric with the axis of rotation. Such compressors ($\alpha$ = 0°) are designated axial-flow compressors and are not considered in this report.

Coordinate system. - Let R and $\theta$ be the dimensionless conical coordinates of a fluid particle relative to the rotating impeller (fig. 2). The conic-radius ratio R is defined as

$$R = \frac{r}{r_T} \tag{1}$$

where

r conic radius (distance along conic element from apex of cone)

Subscript

T impeller tip

The coordinate system (R, $\theta$) rotates with the angular velocity of the impeller $\omega$. A particle of fluid located on this coordinate system is shown in figure 2. The passage-height ratio H of the particle in the direction normal to the conic surface (fig. 2) is a continuous function of the conic-radius ratio R.

$$H = \frac{h}{h_T} = f(R) \tag{2}$$

where h is the passage height at any conic-radius ratio R. The shape of the blades on the conic surface is arbitrary.

Assumptions and limitations. - This analysis assumes that the flow varies only along the surface of the cone, that is, that flow conditions are a function of the two variables R and $\theta$. In order that the assumption of two-dimensional flow on the conic surface be valid, it is necessary that the flow be uniform across the flow passage normal to the conic surface. In order to satisfy this flow condition, it is necessary that: (1) the gradient of h with respect to r be small, and (2) the cone angle $\alpha$ (fig. 1) be sufficiently large. The allowable variation in $\alpha$ from 180° will depend upon the relative magnitudes of h and r and upon the desired accuracy. For the hypothetical limiting case in which the ratio h/r approaches zero everywhere along the conic surface, the analysis is accurate for all values of $\alpha$. In most practical centrifugal compressors, the ratio h/r is smallest near the tip of the impeller; therefore, the analysis is most accurate in the region near the tip.

The assumption of steady flow relative to the impeller applies within the impeller and for the distances upstream and downstream of

the impeller required to set up the boundary conditions. Stationary prerotation vanes (ahead of the impeller) and stationary diffuser vanes (after the impeller) introduce pulsations relative to the rotating impeller and thus make the flow unsteady. However, these pulsations rapidly diminish upstream and downstream of the vanes so that the flow can be treated as steady within the region near the impeller provided the vanes are not too close to the impeller.

Continuity and the stream function. - A fluid particle is shown in figure 2 on a developed view of the conic surface. If $u$ and $v$ are the tangential and "radial" (along the conic element) components, respectively, of the velocity relative to the impeller, then, from continuity considerations for steady flow, the following expression is obtained:

$$\frac{\partial}{\partial R}(\rho v H R) + \frac{\partial}{\partial \theta}(\rho u H) = 0 \tag{3}$$

where $\rho$ is the weight density of fluid.

A dimensionless stream function $\psi$ is defined such that

$$\psi_\theta \equiv \frac{\rho v}{\rho_o c_o} HR \tag{4}$$

and

$$\psi_R \equiv -\frac{\rho u}{\rho_o c_o} H \tag{4a}$$

where

$c$ local speed of sound

Subscript

$o$ absolute inlet stagnation condition

and where the coordinate subscripts ($R$ and $\theta$, in this case) refer to partial derivatives with respect to the coordinates.

The continuity equation (3) then becomes

$$\frac{\partial}{\partial R}\left(c_o\rho_o\psi_\theta\right) - \frac{\partial}{\partial \theta}\left(c_o\rho_o\psi_R\right) = 0$$

or

$$\psi_{\theta R} - \psi_{R\theta} = 0$$



where the double coordinate subscripts ($\theta R$ and $R\theta$, in this case) refer to second partial derivatives with respect to the coordinates. Therefore, the stream function $\psi$ satisfies the continuity condition.

Irrotationality. - In the absence of viscosity, shock, nonuniform heat addition, and so forth, the absolute motion of the fluid particle is irrotational. Therefore, the absolute circulation $\Gamma$ about the particle is zero and, from figure 2,

$$\Gamma = 0 = \frac{\partial}{\partial R}\left[\left(\omega r_T R \sin\frac{\alpha}{2} + u\right) R d\theta\right] dR - \frac{\partial}{\partial \theta}\left(v dR\right) d\theta$$

where $\left(\omega r_T R \sin\frac{\alpha}{2} + u\right)$ is the tangential component of the absolute velocity. After simplification,

$$-2\omega r_T \sin\frac{\alpha}{2} = \frac{u}{R} + \frac{\partial u}{\partial R} - \frac{1}{R}\frac{\partial v}{\partial \theta} \tag{5}$$

Substitution of the stream function $\psi$ as defined by equation (4) gives

$$\frac{2\omega r_T \sin\frac{\alpha}{2}}{\rho_o c_o} = \frac{\psi_R}{\rho H R} + \frac{\partial}{\partial R}\left(\frac{\psi_R}{\rho H}\right) + \frac{1}{R}\frac{\partial}{\partial \theta}\left(\frac{\psi_\theta}{\rho H R}\right)$$

which reduces to

$$2M_T \frac{\rho}{\rho_o} H = \psi_{RR} + \frac{\psi_R}{R} + \frac{\psi_{\theta\theta}}{R^2} - \psi_R \left(\log_e H\right)_R$$

$$- \psi_R \left(\log_e \frac{\rho}{\rho_o}\right)_R - \frac{\psi_\theta}{R^2}\left(\log_e \frac{\rho}{\rho_o}\right)_\theta \tag{6}$$

where the impeller tip Mach number $M_T$ is defined as

$$M_T = \frac{\omega r_T \sin \frac{\alpha}{2}}{c_o} \tag{7}$$

Density ratio. - The general energy equation is used to determine those terms in the differential equation (6) involving the density ratio $\rho/\rho_o$.

$$Jc_pT + \frac{1}{2g}\left[\left(\omega r_T R \sin \frac{\alpha}{2} + u\right)^2 + v^2\right] = Jc_pT_o$$

$$+ \frac{\omega r_T R \sin \frac{\alpha}{2}\left(\omega r_T R \sin \frac{\alpha}{2} + u\right)}{g} - Jc_p\Delta T_w \tag{8}$$

where

$J$ mechanical equivalent of heat

$c_p$ specific heat at constant pressure

$T$ absolute temperature

$g$ acceleration due to gravity

$\Delta T_w$ temperature correction for whirl ahead of impeller

The term

$$\frac{\omega r_T R \sin \frac{\alpha}{2}\left(\omega r_T R \sin \frac{\alpha}{2} + u\right)}{g}$$

is the work done by the impeller upon the fluid particle if the fluid particle possesses no whirl (radius, $r \sin \alpha/2$, times tangential component of absolute velocity) ahead of the impeller, and the term

$$Jc_p\Delta T_w = \frac{\omega r_T R_I \sin \frac{\alpha}{2}\left(\omega r_T R_I \sin \frac{\alpha}{2} + u_I\right)}{g} \tag{8a}$$

is the reduction in work that results from the whirl ahead of the impeller. The subscript I refers to impeller inlet. These same expressions for the work done apply in the vaneless portion of the diffuser, where the tangential component of the relative velocity $u$ decreases (takes on larger negative values) in such a manner that the work terms remain constant.

Rearrangment of equation (8) and solution for the temperature ratio $T/T_o$ results in

$$\frac{T}{T_o} = 1 + \frac{\gamma-1}{2}\left[(RM_T)^2 - \left(\frac{q}{c_o}\right)^2\right] - \frac{\Delta T_w}{T_o} \tag{9}$$

where

$\gamma$ ratio of specific heats

$q$ velocity relative to impeller

$$q = \sqrt{u^2 + v^2} \tag{10}$$

From equation (8a), the correction term in equation (9) for the whirl ahead of the impeller becomes

$$\frac{\Delta T_w}{T_o} = (\gamma-1)\, R_I M_T \left[R_I M_T + \left(\frac{u}{c_o}\right)_I\right] \tag{9a}$$

For an isentropic process, the density ratio is related to the temperature ratio by

$$\frac{\rho}{\rho_o} = \left(\frac{T}{T_o}\right)^{\frac{1}{\gamma-1}}$$

so that

$$\frac{\rho}{\rho_o} = \left\{1 + \frac{\gamma-1}{2}\left[(RM_T)^2 - \left(\frac{q}{c_o}\right)^2\right] - \frac{\Delta T_w}{T_o}\right\}^{\frac{1}{\gamma-1}} \tag{11}$$

Also, from equations (10) and (4),

$$\frac{\rho q}{\rho_o c_o} = \left[\left(\frac{\psi_R}{H}\right)^2 + \left(\frac{\psi_\theta}{HR}\right)^2\right]^{\frac{1}{2}} \tag{12}$$

Equations (11) and (12) together with the general differential equation (6) provide three equations with three unknowns: $\psi$, $q/c_o$, and $\rho/\rho_o$. The solution of these equations determines the steady flow of compressible fluid through centrifugal compressors

with arbitrary blade shapes, with arbitrary variations in the passage-height ratio, and with a constant cone angle. Equation (6), which is nonlinear, can be solved (together with equations (11) and (12)) by relaxation methods.

Relaxation methods. - The relaxation solution of the differential equation determines the value of $\psi$ at each point of a grid placed within the boundaries of the problem. Values of $\psi$ are first assumed, and the residuals $Q$, which result from the assumed values of $\psi$, are computed for each point of the grid by expressing the differential equation (for example, equation (6)) in finite-difference form with the sum of all terms equal to $Q$ instead of zero. The final solution is obtained by systematically varying (relaxing) the interior values of $\psi$ until the values of $Q$ at each grid point approach zero. For the numerical solution of this problem by relaxation methods, it is convenient to transform the $R,\theta$ coordinates so that the arbitrary blade shapes become straight and parallel, thus a grid of equally spaced points between the blades is possible (reference 8, p. 13).

Transformation of coordinates. - The transformation of coordinates is given by the analytic function

$$f(z) = f(Re^{i\theta}) = \xi(R,\theta) + i\eta\ (R,\theta) \qquad (13)$$

where $z$ is a complex variable and the $\xi$ and $\eta$ coordinates (Cartesian coordinates in transformed plane) are the velocity potential lines ($\xi$ = constant) and streamlines ($\eta$ = constant) in the physical $R\theta$-plane for incompressible flow through the stationary impeller ($\omega = 0$) with constant passage height ($H = 1$). It is convenient to choose the $\xi$, $\eta$ coordinates to correspond to smooth (shockless) inlet and exit conditions with respect to the impeller blades.

The transformation results in straight parallel lines for the impeller-blade boundaries as these boundaries correspond to constant values of the incompressible stream function $\eta$. The $\xi$, $\eta$ coordinates are given for certain blade shapes by simple analytic expressions (p. 17) but, for arbitrary blade shapes, it is convenient to solve the well-known differential equations for the incompressible stream function and velocity potential by relaxation methods (reference 8).

Equation (6) is now expressed in terms of the new variables $\xi$ and $\eta$. This change of variables is described in appendix B with the following result:

$$\frac{2M_T}{q_i^2}\frac{\rho}{\rho_o}H = \psi_{\xi\xi} + \psi_{\eta\eta} - \psi_\xi\left(\log_e\frac{\rho}{\rho_o}\right)_\xi - \psi_\eta\left(\log_e\frac{\rho}{\rho_o}\right)_\eta$$

$$-\frac{1}{q_i^2}\left(\psi_\xi v_i - \psi_\eta u_i\right)\left[(\log_e H)_\xi\, v_i - (\log_e H)_\eta\, u_i\right] \qquad (14)$$

where $H$ is now a function of $\xi$ and $\eta$ and

$q_i$ velocity for incompressible flow relative to stationary impeller with constant blade height ($R\theta$-plane)

$u_i$, $v_i$ tangential and radial components of velocity $q_i$, respectively

The incompressible velocities $u_i$, $v_i$, and $q_i$ are related to the incompressible stream function $\eta$ by the following equations:

$$u_i = -\eta_R \qquad (15)$$

$$v_i = \frac{\eta_\theta}{R} \qquad (15a)$$

$$q_i = \sqrt{\eta_R^2 + \frac{\eta_\theta^2}{R^2}} \qquad (15b)$$

Equation (14) is the general differential equation expressed in $\xi,\eta$ coordinates for the flow of compressible fluid through centrifugal compressors with arbitrary blade shapes, with arbitrary variations in the passage-height ratio, and with constant cone angles.

Also, equation (12) in terms of the transformed coordinates $\xi$ and $\eta$ (see equations (46) and (47) in appendix B) becomes

$$\frac{\rho q}{\rho_o c_o} = \frac{q_i}{H}\left(\psi_\xi^2 + \psi_\eta^2\right)^{\frac{1}{2}} \qquad (16)$$

where $H$ is a function of $\xi$ and $\eta$.

Finite-difference equation. - In order to solve the system of equations (equations (11), (14), and (16)) by relaxation methods, equations (14) and (16) must first be changed to finite-difference form. This change is accomplished with the aid of the following equations (reference 7, p. 19):

$$\left.\begin{aligned} F_{\xi} &\approx \frac{1}{2b}(F_1 - F_3) \\ F_{\eta} &\approx \frac{1}{2b}(F_4 - F_2) \\ F_{\xi\xi} &\approx \frac{1}{b^2}(F_1 + F_3 - 2F) \\ F_{\eta\eta} &\approx \frac{1}{b^2}(F_2 + F_4 - 2F) \end{aligned}\right\} \qquad (17)$$

where

F any twice-differentiable function of variables $\xi$ and $\eta$

b grid spacing

Subscripts

1, 2, 3, 4 four points adjacent to grid point being considered (F with no subscript)

A sample grid is shown in figure 3. The grid spacing b is arbitrary. However, the smaller the value of b, that is, the larger the number of grid points, the greater is the accuracy of the approximate, finite-difference equations (17).

With the aid of equations (17), equation (14) becomes

$$\psi_1 + \psi_2 + \psi_3 + \psi_4 - 4\psi - \frac{(\psi_1 - \psi_3)}{4}\left(\log_e \frac{\rho_1}{\rho_o} - \log_e \frac{\rho_3}{\rho_o}\right)$$

$$- \frac{(\psi_4 - \psi_2)}{4}\left(\log_e \frac{\rho_4}{\rho_o} - \log_e \frac{\rho_2}{\rho_o}\right) = \frac{1}{4q_1^2}\left[(\psi_1 - \psi_3)\, v_1\right.$$

$$\left. - (\psi_4 - \psi_2)\, u_1\right]\left[(\log_e H_1 - \log_e H_3)\, v_1 - (\log_e H_4 - \log_e H_2)\, u_1\right]$$

$$- \frac{2M_T}{q_1^2}\frac{\rho}{\rho_o} Hb^2 = Q \qquad (18)$$

Equation (18) is the finite-difference equation used to compute the residual $Q$ at each grid point from the estimated values of $\psi$ at the adjacent grid points.

Equation (16) in finite-difference form becomes

$$\frac{\rho q}{\rho_o c_o} = \frac{q_1}{2bH}\left[(\psi_1 - \psi_3)^2 + (\psi_4 - \psi_2)^2\right]^{\frac{1}{2}} \qquad (19)$$

The density ratios in equation (18) can now be determined in the following manner: From equation (11), for fixed values of $RM_T$, curves of $\log_e \rho/\rho_o$ plotted against $\rho q/\rho_o c_o$ can be computed for a constant value of $\Delta T_w/T_o$. These curves have been plotted in figure 4 for $\Delta T_w/T_o$ equal to zero, that is, for the case in which there is no

whirl in the fluid ahead of the impeller. The logarithm of the density ratio $\log_e \rho/\rho_o$ at each point on the grid is therefore determined by first obtaining the flow-rate ratio $\rho q/\rho_o c_o$ from equation (19) after which $\log_e \rho/\rho_o$ can be obtained from plots of equation (11), such as figure 4.

Boundary considerations. - The solution of equation (18) depends upon the boundary values of the stream function $\psi$, which are determined from the compressor design characteristics and operating conditions. The boundary values of $\psi$ along the blade surfaces can be determined from the following considerations.

The differential flow rate between adjacent streamlines is shown in figure 5. The radial component of the flow rate is

$$\rho v h_T r_T H R d\theta$$

and the tangential component of the flow rate is

$$- \rho u h_T r_T H dR$$

The differential flow rate is therefore given by

$$dw = \rho v h_T r_T H R d\theta - \rho u h_T r_T H dR$$

where $w$ is the flow rate between streamlines. From equations (4a) and (4b),

$$dw = \rho_o c_o h_T r_T \left(\psi_\theta d\theta + \psi_R dR\right)$$

but

$$d\psi = \psi_\theta d\theta + \psi_R dR$$

Therefore

$$dw = \rho_o c_o h_T r_T d\psi \tag{20}$$

or

$$\Delta w = \rho_o c_o h_T r_T \Delta\psi \tag{20a}$$

From equation (20a), the stream function $\psi$ must be constant along the blade surfaces (because the flow rate between blades is constant).

By definition, the driving face of a blade is the face in the direction of rotation, and the trailing face is the opposite side of the blade. Integration of equation (20) across the impeller passage from the driving face of one blade and the arbitrary setting of $w$ and $\psi$ equal to zero along the driving face results in

$$w = \rho_o c_o h_T r_T \psi \tag{21}$$

The value of $\psi$ at any point in the flow field is therefore a measure of the flow rate between the streamline at that point and the driving face of the impeller blade. In particular, along the trailing face of a blade, $\psi$ is constant and equal to $\psi_t$ where the subscript $t$ refers to the trailing face, and $w$ is equal to $W/B$ where $W$ is the compressor (total) flow rate and $B$ is the number of compressor passages (or blades).

Equation (21) then becomes

$$\frac{W}{B} = \rho_o c_o h_T r_T \psi_t \tag{22}$$

This equation can be simplified by the following considerations:

The flow area at the impeller tip $a_T$ is given by

$$a_T = B\sigma_T r_T h_T \tag{23}$$

where $\sigma$ is the included angle of the passage defined by

$$\sigma = \theta_t - \theta_d \tag{24}$$

where the subscript $d$ refers to the driving face of a blade. Combining equations (22) and (23) to eliminate $Bh_T r_T$ results in

$$\frac{W}{\rho_o a_T c_o} = \frac{\psi_t}{\sigma_T}$$

The boundary value of $\psi$ along the trailing face of the blade is therefore given by

$$\psi_t = \varphi\sigma_T \tag{25}$$

where the flow coefficient $\varphi$ is defined as

$$\varphi = \frac{W}{\rho_o a_T c_o} \tag{26}$$

The boundary values of $\psi$ in the diffuser are determined from the Kutta condition, which requires that the streamline along the blade surface in the impeller be tangent to the blade at the tip. The effect of the Kutta condition on the boundary values in the diffuser will be discussed later in connection with the numerical example of this report.

The boundary values of $\psi$ ahead of the inlet to the impeller depend upon the whirl of the fluid approaching the inlet. This whirl determines the gradients of $\psi$ with respect to $\xi$ and $\eta$ along the boundaries rather than the values of $\psi$ itself. If the flow for smooth entry is desired, this condition can be obtained in essentially the same way as the Kutta condition at the outlet. The whirl ahead of the inlet is then uniquely determined by the smooth inlet condition.

Equivalent mixed-flow compressors. - As previously stated, this analysis applies to mixed-flow compressors with any fixed cone angle including the special case of the radial-discharge compressor in which the cone angle is 180°. However, as a result of the assumption in this analysis that the flow varies only along the conic surface, which can be developed into a plane (fig. 2), the solution obtained for a given fixed cone angle also applies to certain other mixed-flow compressors with a fewer or greater number of like passages with the same included passage angles, blade-thickness distributions, and so forth. For example, the included angle of the developed view of a mixed-flow compressor (fig. 2) is given by (assuming the blade thickness at the tip is zero)

$$2\pi \sin\frac{\alpha}{2} = B\sigma_T$$

which, for a radial-discharge compressor ($\alpha$ = 180°) with 20 blades (for example), becomes

$$2\pi = 20\,\sigma_T$$

The ratio of these equations results in an expression for the mixed-flow cone angle $\alpha$ as a function of the number of impeller flow passages that are similar to the flow passages (20) in the radial-discharge impeller

$$\alpha = 2 \sin^{-1} \frac{B}{20} \tag{27}$$

From equation (27), the mixed-flow compressor cone angle $\alpha$ has been computed for several values of B and the results are given in the following table:

| Cone angle, $\alpha$ (deg) | Number of passages, B |
|---|---|
| 180 (radial) | 20 |
| 143.6 | 19 |
| 128.4 | 18 |
| 116.4 | 17 |

The flow in a mixed-flow compressor is therefore equivalent to the flow in a radial-discharge compressor with a greater number of blades (but with the same included passage angles $\sigma$). Increasing the number of blades in a radial-discharge compressor decreases the blade loading and the maximum local Mach number and increases the impeller slip factor. The blade loading and the maximum local Mach number are therefore less and the slip factor is greater for a mixed-flow compressor than for a radial-discharge compressor with the same number of blades (because $\sigma$ is less for the mixed-flow compressor).

Equivalent inward-flow turbines. - The reversal of the flow direction through a centrifugal compressor and the reversal of the direction of impeller rotation results in an inward-flow turbine. The general analysis presented in this report therefore also applies to inward-flow turbines with arbitrary blade shapes, with arbitrary variations in the passage-height ratio, and with constant cone angles. In fact, any solution obtained for a centrifugal compressor with smooth (shockless) entry is also a solution (with the flow direction and the impeller rotation direction reversed) for an inward-flow turbine with shockless entry. The shockless entry for the compressor corresponds to the Kutta condition for the turbine and vice versa.

## Particular Case - Thin Logarithmic-Spiral Blades

In the general case of this analysis, the differential equations governing the flow through compressors with arbitrary blade shapes have been developed in terms of the transformed coordinates $\xi$ and $\eta$, which can be determined by relaxation methods.

In the particular case of this analysis, a simple analytic expression that determines a particular thin-blade shape is considered. Such an analytic expression is desirable because it specifies the transformed coordinates $\xi$ and $\eta$ in terms of $R$ and $\theta$ and therefore eliminates the additional relaxation solution otherwise required to obtain $\xi$ and $\eta$.

Logarithmic-spiral blades. - This class of blade is given by the analytic function

$$\begin{aligned} f(z) &= (N + iK) \log_e z \\ &= (N + iK) \log_e (Re^{i\theta}) \\ &= (N + iK)(\log_e R + i\theta) \\ &= (N \log_e R - K\theta) + i (K \log_e R + N\theta) \end{aligned} \tag{28}$$

where $N$ and $K$ are constants to be determined by boundary conditions. From equations (13) and (28),

$$\xi = N(\log_e R - \frac{K}{N} \theta) \tag{29}$$

$$\eta = N(\frac{K}{N} \log_e R + \theta) \tag{29a}$$

Any incompressible streamline ($\eta$ = constant) or portion thereof may be replaced by an infinitely thin blade without disturbing the flow pattern. Equation (29a) with $\eta$ constant therefore represents a thin-blade shape. Any number of blades may be selected corresponding to different constant values of $\eta$.

The constants $N$ and $K$ are determined in appendix C from the boundary conditions,

$$\eta = \psi_t$$

when

$$\theta = \sigma_T$$

and

$$R = 1.0$$

(from which the zero point for $\theta$ is at the tip of the driving face of the blade). Equations (29) and (29a) become

$$\xi = \varphi (\log_e R + \theta \tan \beta) \tag{30}$$

$$\eta = \varphi (\theta - \tan \beta \log_e R) \tag{30a}$$

where $\beta$ is the blade curvature angle between conic-radius ratio R and tangent to blade surface (fig. 6).

The blade shape in the $R\theta$-plane is given by equation (30a), which, with $\eta$ constant, determines a logarithmic spiral (fig. 6). In appendix C, the angle $\beta$ is shown to be constant for a given logarithmic spiral. For positive values of $\beta$, the blades are curved forward (in the direction of rotation); for negative values of $\beta$, the blades are curved backward; and for $\beta$ equal to zero, the blades are straight and radial along conic radii (fig. 6).

Equations (30) and (30a) relate every point in the $R\theta$-plane to a corresponding point in the $\xi\eta$-plane. Solving these equations for R and $\theta$ in terms of $\xi$ and $\eta$

$$R = e^{\frac{\xi - \eta \tan \beta}{\varphi \sec^2 \beta}} \tag{31}$$

$$\theta = \frac{\eta + \xi \tan \beta}{\varphi \sec^2 \beta} \tag{31a}$$

In terms of the particular transformed coordinates given by equations (30) and (30a), the differential equation for the flow of compressible fluid through centrifugal compressors with logarithmic-spiral blades becomes

$$2M_T \frac{\rho}{\rho_o} H \frac{e^{\frac{2(\xi - \eta \tan \beta)}{\varphi \sec^2 \beta}}}{(\varphi \sec \beta)^2} = \psi_{\xi\xi} + \psi_{\eta\eta} - \psi_\xi \left(\log_e \frac{\rho}{\rho_o}\right)_\xi - \psi_\eta \left(\log_e \frac{\rho}{\rho_o}\right)_\eta$$

$$- (\psi_\xi \cos \beta - \psi_\eta \sin \beta) \left[(\log_e H)_\xi \cos \beta - (\log_e H)_\eta \sin \beta\right] \quad (32)$$

Passage-height ratio H. - Instead of the arbitrary function for the passage-height ratio given by equation (2), let the variation in H be given by

$$H = R^m \quad (33)$$

where m is an arbitrary exponent.

If $\sigma$ equals $\sigma_T$ for all values of R, the variation in the flow-area ratio with R becomes, from equations (23) and (33),

$$A = \frac{a}{a_T} = \frac{B\sigma_T r h}{B\sigma_T r_T h_T} = RH = R^{m+1} \quad (34)$$

where A is the flow-area ratio. This relation between A and R is plotted in figure 7 for several values of the exponent m. For m equal to zero, the passage height remains constant; for m equal to -1, the passage area remains constant.

For logarithmic-spiral blades, equation (31) is combined with equation (33) and the passage-height ratio H becomes

$$H = e^{\frac{m(\xi - \eta \tan \beta)}{\varphi \sec^2 \beta}} \tag{33a}$$

from which equation (32) reduces to

$$2M_T \frac{\rho}{\rho_o} \frac{e^{\frac{(m+2)(\xi - \eta \tan \beta)}{\varphi \sec^2 \beta}}}{(\varphi \sec \beta)^2} = \psi_{\xi\xi} + \psi_{\eta\eta} - \psi_\xi \left(\log_e \frac{\rho}{\rho_o}\right)_\xi$$

$$- \psi_\eta \left(\log_e \frac{\rho}{\rho_o}\right)_\eta - \frac{m}{\varphi \sec^2 \beta} (\psi_\xi - \tan \beta \, \psi_\eta) \tag{35}$$

Straight radial blades. - For straight blades along conic radii, the blade angle $\beta$ is zero (fig. 6) and equation (35) reduces to

$$2M_T \frac{\rho}{\rho_o} \frac{e^{\frac{(m+2)\xi}{\varphi}}}{\varphi^2} = \psi_{\xi\xi} + \psi_{\eta\eta} - \psi_\xi \left(\log_e \frac{\rho}{\rho_o}\right)_\xi$$

$$- \psi_\eta \left(\log_e \frac{\rho}{\rho_o}\right)_\eta - \frac{m}{\varphi} \psi_\xi \tag{36}$$

Incompressible flow. - For incompressible flow, $\rho/\rho_o$ is equal to 1.0 and equation (36) becomes

$$2M_T \frac{e^{\frac{(m+2)\xi}{\varphi}}}{\varphi^2} = \psi_{\xi\xi} + \psi_{\eta\eta} - \frac{m}{\varphi} \psi_\xi \tag{37}$$

where $M_T$ is now a fictious tip Mach number based upon a constant fictious speed of sound, which also appears in the definitions of $\psi$, $\xi$, $\eta$, and $\varphi$.

Constant blade height. - For constant blade height, the exponent $m$ is zero (equation (33)) and equation (37) reduces to

$$2M_T \frac{e^{\frac{2\xi}{\varphi}}}{\varphi^2} = \psi_{\xi\xi} + \psi_{\eta\eta} \tag{38}$$

Detailed solutions to this equation (in slightly altered form) have been obtained by a number of investigators. (For example, reference 1.)



Summary of equations. - Special forms of the basic differential equation (14) for steady flow through conical centrifugal compressors have been developed for various designs and operating conditions. The equations are listed in the following table:

| Equation | Blade shape | Passage height | Flow |
|---|---|---|---|
| (32) | Logarithmic spiral | $H = f(R)$ | Compressible |
| (35) | Logarithmic spiral | $H = R^m$ | Compressible |
| (36) | Straight | $H = R^m$ | Compressible |
| (37) | Straight | $H = R^m$ | Incompressible |
| (38) | Straight | $H$ = constant | Incompressible |

These differential equations express the stream function $\psi$ as a function of the transformed coordinates $\xi$ and $\eta$. The equations are changed to finite-difference form and solved by relaxation methods. This form is obtained with the aid of equations (17) and has been obtained for equation (14), the finite-difference form of which is given by equation (18). The density ratio $\rho/\rho_o$ is determined from figure 4 or from equation (11) with the aid of equation (19) in which the parameter $q_1$ is obtained from equations (10) and (47) or from equation (52b) in appendix C and in which the variable $H$ is a given function of $R$ (which is related to $\xi$ and $\eta$).

## NUMERICAL PROCEDURE

A detailed outline of the numerical procedures for the relaxation solution of compressible-flow problems is given in reference 8. The emphasis is placed herein on those features of the solution that are peculiar to the flow in centrifugal compressors.

The solution of each differential equation developed for the stream function $\psi$ (equations (14), (32), (35), (36), (37), and (38)) requires special treatment depending upon the compressor design characteristics and the flow conditions that the equation represents. However, the numerical procedure is in many respects similar for all equations. The remainder of this section will therefore be concerned with the numerical solution of equation (36), which is the equation used in the numerical example of this report (straight thin blades along conic radii).

Parameters. - An inspection of the differential equation for the stream function $\psi$ (equation (36)), together with the auxiliary equations (7), (9a), (11), and (25), indicates eight parameters, which, together with the blade angle $\beta$ (equal to zero in equation (36)), specify the design characteristics and operating conditions of the compressor.

Design parameters:

(1) Passage-height exponent $m$, which relates passage-height ratio $H$ to conic-radius ratio $R$

$$H = R^m \tag{33}$$

In the more general case, $H$ can be given as an arbitrary function of $R$.

(2) Cone angle $\alpha$, which is constant (fig. 1)

(3) Blade curvature angle $\beta$, which for a logarithmic-spiral blade remains constant and for straight blades (along conic radii) is equal to zero

(4) Included angle of impeller passage on conic surface $\sigma$, which is measured from driving face of one blade to trailing face of next blade

(5) Inlet conic-radius ratio $R_I$, which is ratio of blade-inlet conic radius to blade-tip conic radius

(6) Initial whirl of fluid ahead of impeller, which is designated by ratio $\Delta T_w/T_o$ and which is determined by design configuration of compressor ahead of impeller and by flow rate (operating parameter) through compressor

Operating parameters:

(7) Tip Mach number $M_T$, which is defined as

$$M_T = \frac{\omega r_T \sin\frac{\alpha}{2}}{c_o} \tag{7}$$

(8) Flow coefficient $\varphi$, which is defined as

$$\varphi = \frac{W}{\rho_o a_T c_o} \tag{26}$$

For a given compressor, this coefficient is easily shown to be proportional to standard equivalent-flow-rate parameter $W\sqrt{\theta}/\delta$ (reference 9)

where

$\theta$ ratio of inlet stagnation temperature to standard sea-level temperature

$\delta$ ratio of inlet stagnation pressure to standard sea-level pressure

(9) Ratio of specific heats $\gamma$, which determines variation in density ratio $\rho/\rho_o$ as given by equation (11)

Boundary conditions. - The boundary values of the stream function $\psi$ are determined by the parameters previously outlined and by the Kutta condition for tangency of flow at the blade tip. The various boundary values of $\psi$ are shown on the relaxation grid in figure 8. The manner in which these boundary values are obtained is summarized as follows:

(1) The value of the stream function along the driving face of the blade $\psi_d$ (fig. 8) is arbitrarily set equal to zero. (See p. 14.)

(2) The value of the stream function along the trailing face of the blade $\psi_t$ (fig. 8) is constant and is given by

$$\psi_t = \varphi\sigma_T \tag{25}$$

(3) The values of the stream function along the boundaries ahead of the impeller-blade inlet depend (among other things) upon the inlet design parameters $R_I$ and $\Delta T_w/T_o$. For the particular case (used in the numerical example) of straight blades ($\beta = 0$) extended to the origin, at which a point source is assumed (p. 27), the values of $R_I$ and $\Delta T_w/T_o$ are zero and the left bound of the relaxation grid (fig. 8) is located at some radius ratio R within the impeller passage. The value of the stream function along the left bound $\psi_l$ (fig. 8) is computed for this particular case from equation (41). This equation has been found to be quite accurate for values of $R = f(\xi)$ less than 0.65. (See p. 32.)

(4) The values of the stream function along the upper bound of the diffuser $\psi_e$ (fig. 8) are estimated by equation (54) developed in appendix D. These estimated values of $\psi_e$ are corrected by the relaxation methods to be subsequently discussed.

The value of the stream function at the upper right corner of the grid $\psi_r$ (fig. 8) is first determined by the estimated values of $\psi_e$. However, to satisfy the Kutta condition, the value of $\psi_r$ must be of such a magnitude that the flow leaves tangent to the blade surface at the blade tip. If the resulting relaxation solution for the streamline configuration in the compressor does not satisfy the Kutta condition, a new value of $\psi_r$ is selected, the estimated values of $\psi_e$ adjusted accordingly, and the solution repeated as many times as is necessary.

(5) The values of the stream function along the lower bound of the diffuser $\psi_f$ (fig. 8) are, from symmetry considerations, $\psi_t$ less than $\psi_e$.

$$\psi_f = \psi_e - \psi_t \tag{39}$$

(6) The values of the stream function along the right bound of the relaxation grid are determined by $\psi_r$ and by the assumption that, along this bound, $\Delta\psi/\Delta\eta$ is a constant. For the numerical example, this assumption has been found to be accurate enough for values of $R = f(\xi)$ somewhat greater than 1.20.

Grid layout. - Having determined the values of $\psi$ at each point on the grid boundary, the values of $\psi$ at each of the interior points is estimated and recorded upon the grid sheet (fig. 8), which should be sufficiently large to accommodate the calculations required by the relaxation procedure. After estimating

the interior values of $\psi$, the problem resolves itself into two parts: (1) calculation of the residual Q resulting from the estimated values of $\psi$, and (2) relaxation (elimination) of the residual by suitable adjustments in the estimated values of $\psi$.

Residuals. - In order to determine the residual at each point of the grid system, the partial differential equation (for example, equation (36)) is expressed in finite-difference form by methods outlined in the analysis. All terms of the equation are placed equal to the residual Q, as has been done in equation (18). The terms involving the density ratio $\rho/\rho_o$ are determined from figure 4 or equation (11) with the aid of equation (19). In order to determine the value of the density ratio at the boundary points in the impeller, it is necessary to extrapolate the values of the stream function $\psi$ by graphical or numerical methods to obtain the velocities at the boundary. In the diffuser, however, this extrapolation is not required because the values of $\psi$ repeat themselves in a continuous manner from passage to passage. If the estimated values of $\psi$ at all grid points are correct, the value of Q is zero at all points. If, however, the estimated values of $\psi$ are incorrect, the values of Q are finite and may be positive or negative.

Relaxation. - With the residuals at each of the grid points computed, it remains to relax (that is, reduce) these residuals by suitable changes in the values of $\psi$. In order to determine the magnitude of the required changes in $\psi$, all terms of the finite-difference equation (equation (18), for example) are assumed to remain constant except the term $4\psi$. A change in the value of $\psi$ will therefore cause a four-fold change of opposite sign in the value of Q. This change in the value of $\psi$ will also cause an equal change in the values of Q at each of the adjacent grid points (fig. 3). These changes in $\psi$ and Q are recorded on the grid sheet as the work progresses. By continually relaxing the larger residuals any desired amount, the values of all residuals gradually approach zero. When this condition is reached, the residuals are recomputed using the finite-difference equation and taking into account the new values of the density ratio. When the new values of Q have been computed, the relaxation procedure is repeated as often as necessary to achieve the desired accuracy.

Accuracy. - No quantitative evaluation of the accuracy of relaxation solutions is available (reference 10, p. 176). However, because the computed velocities (and pressures) depend upon differences in the values of the stream function $\psi$ at adjacent grid

points, that is, the small difference of large numbers, it is important to know the values of $\psi$ with sufficient accuracy to assure the desired accuracy for the pressure and velocity calculations. In this report, the values of $\psi$ were computed to the nearest 0.0001 compared with the maximum value of $\psi$ at the trailing face of the blade of 0.1570. The resulting values of pressure and velocity are estimated to be accurate within 1 or 2 percent.

Final solution. - The streamline configuration can be determined from the final values of $\psi$ at each of the grid points. (Streamlines are lines of constant $\psi$.) If the streamline leaving the tip of the impeller is tangent to the blade at the tip, the estimated value of $\psi_r$ (p. 24) is correct; otherwise a new value of $\psi_r$ must be selected and the entire solution repeated.

After the correct distribution of $\psi$ on the grid is obtained, the pressure distribution can be determined from the density distribution and the Mach number distribution can be determined from equation (19), the density ratio, and the speed of sound ratio $c/c_o$, which is related to the density ratio by

$$\frac{c}{c_o} = \left(\frac{\rho}{\rho_o}\right)^{\frac{\gamma-1}{2}}$$

From the preceding information, such quantities as the impeller slip (appendix E), the boundary-layer growth, and the blade loading can be estimated.

## NUMERICAL EXAMPLE

Design and operating parameters. - A numerical example has been computed for the following design and operating parameters:

Design parameters:

(1) Constant flow area, $m$ . . . . . -1
(2) Cone angle, $\alpha$, degrees . . . . . 180
(3) Straight blades along conic radii, $\beta$ . . . . . 0
(4) Included passage angle, $\sigma = \sigma_T$ . . . . . $2\pi/20$
(20 thin blades)
(5) Inlet conic-radius ratio, $R_I$ . . . . . 0
(6) Initial whirl of fluid approaching impeller inlet, $\Delta T_w/T_o$ . . . . . 0

Operating parameters:
(7) Tip Mach number, $M_T$ . . . . . 1.5
(8) Flow coefficient, $\varphi$ . . . . . 0.5
(9) Ratio of specific heats, $\gamma$ . . . . . 1.4



In order to insure steady-flow conditions, a vaneless diffuser has been selected although a vaned diffuser located far enough downstream of the impeller would also be satisfactory. (See p. 5) A diagram of the impeller and the vaneless diffuser is shown in figure 9. The passage-height ratio H varies in such a manner that the radial-flow area remains constant. The straight impeller blades are extended radially inward to the center where a point source has been assumed. A point source at the center of the impeller or a circular line source at some conic-radius ratio R must be assumed in the two-dimensional analysis in order to supply the impeller with the necessary flow rate. In this example, the straight blades have been extended to the center ($R_I = 0$) to obtain smooth (shockless) entry to the straight blades (without providing inlet whirl). In practice, smooth entry to straight blades without inlet whirl is obtained by curved inducer vanes involving flow that is not along a conic surface.

The results of the numerical example are presented in figures 10 to 15. These figures are discussed.

Streamlines. - The streamline configuration relative to the rotating impeller is shown in figure 10. The grid lines on the figure indicate the grid spacing used to obtain the final relaxation solution. The streamlines are designated in such a manner that the value of the streamline indicates the percentage of flow through the passage that lies between the streamline and the driving face of the blade (right side of passage). For example, 20 percent of the flow through the passage lies between the streamline 0.2 and the driving face. It is interesting to note that 20 percent of the flow occupies more than 50 percent of the flow area at a radius ratio of 0.86. The spacing of the streamlines is indicative of the velocities in the compressor; the smaller the spacing, the higher the velocity. The highest velocities therefore occur along the trailing face of the blade, the lowest velocities near the driving face.

As a result of the irrotationality of the absolute fluid motion in the vaneless diffuser, the absolute tangential velocity of the fluid decreases as the radius ratio R increases. The tangential velocity of the fluid relative to the rotating $R,\theta$ coordinate

system therefore, decreases rapidly (takes on large negative values) in the diffuser and the relative streamlines in the diffuser are steeply sloped in the direction opposite to the impeller rotation, as shown in figure 10.



Eddy formation. - For the design and operating conditions of this example, a wheel-type eddy forms on the driving face of the blade (fig. 10). This eddy is attached to the blade and rotates with an angular velocity equal and opposite to the rotational velocity of the impeller $\omega$. (The motion is not a simple rotation but a combination of rotation and deformation required to satisfy boundary conditions.) Such eddies form at low flow rates and result from the condition of irrotationality relative to an absolute system of coordinates.

An expanded view of the eddy is shown in figure 11. The flow rate within the eddy amounts to less than 2 percent of the flow rate through the impeller (as indicated by the designation of the streamlines). This low flow rate indicates low velocities within the eddy.

It appears that, in an actual compressor under the influence of viscous shearing forces, the size and the position of the eddy might be unsteady. Under these conditions, the pressure forces are not in equilibrium and the flow is unstable. It may therefore be desirable to eliminate the eddy by proper changes in the design and the operating conditions of the compressor.

The eddy can be eliminated by the following methods: When the flow rate through the rotating impeller is zero, the eddy occupies the entire flow passage (reference 1, p. 1000). The eddy is therefore reduced and finally eliminated by increasing the flow rate through the impeller. The increase in the flow rate, however, is limited by choke in the compressor. In this event, it may be desirable to replace the eddy by a solid plug of light material attached to the impeller blade and disk.

Kutta condition. - Generally, several attempts are required to satisfy the Kutta condition. The second attempt is shown in figure 12(a). This figure is an expanded view of the region in the vicinity of the blade tip. Streamline 1.0 does not leave tangent to the blade tip. In this case, to satisfy the Kutta condition of tangency, it is necessary to reduce the circulation around the compressor by increasing the assumed value of $\psi_r$. (See fig. 8 and p. 24.)

The third attempt to satisfy the Kutta condition is shown in figure 12(b). Streamline 1.0 is very nearly tangent to the blade tip. This solution was considered satisfactory.

1015

Slip. - The computed values of the slip factor (appendix E) as determined from the streamline configuration were 0.91 for the second attempt to satisfy the Kutta condition and 0.90 for the third (final) attempt.

Constant Mach number lines. - Lines of constant Mach number relative to the impeller are shown in figure 13. A maximum local Mach number in the impeller of 0.64 occurs on the trailing face of the blade at a radius ratio of 0.68.

The maximum relative Mach number at the impeller tip is less than 0.30. The low relative Mach numbers at the tip result from the high tip speed of the impeller, which increases the density and therefore reduces the velocity.

The somewhat irregular velocity profile at the impeller tip becomes quite uniform within 6 to 8 percent of the impeller radius beyond the tip. This rapid adjustment of the flow indicates that, provided the absolute leaving velocity is subsonic, vaned diffusers can be located quite close to the impeller tip without appreciable losses resulting from poor (unsteady) velocity distribution relative to the stationary diffuser vanes. However, in the presence of boundary layer and separation, the velocity profile would be considerably more irregular than obtained in this solution. The relatively close spacing of the Mach number lines along the trailing face of the blade near the tip indicates rapidly decelerated flow, which is conducive to boundary-layer separation.

Constant-pressure-ratio lines. - Lines of constant pressure ratio are shown in figure 14. Within the impeller, the pressures on the driving face of the blade are higher than the pressures on the trailing face. This difference in pressure across the blade accounts for the impeller torque.

An expanded view of the pressure ratios in the vicinity of the blade tip is shown in figure 15. As a result of the Kutta condition, the pressures (and the velocities) are equal on both sides of the blade tip. This unloading at the blade tip decreases the impeller work and therefore decreases the impeller slip factor.

## SIMPLIFIED ANALYSIS

The relaxation solution presented in this report is lengthy. It would therefore be advantageous to have a quicker, although less accurate, means of estimating the flow conditions within the impeller. In this section, a simplified analysis developed in appendix F for radial-discharge and mixed-flow impellers with straight blades (along conic radii) is discussed.



Velocity distribution. - The simplified analysis is based on the assumption that the tangential component of the velocity relative to the impeller is zero at all radii within the impeller. This simplified analysis includes blades of varying thickness provided the variation is not sufficiently great to result in appreciable values of the tangential component of velocity to the impeller u. The irrotationality equation (5) reduces to

$$2\omega r_T \sin\frac{\alpha}{2} = \frac{1}{R}\frac{\partial v}{\partial \theta}$$

which, when integrated between limits, and so forth, becomes

$$\frac{v}{c_o} = \frac{v_d}{c_o} + 2RM_T\,\theta \tag{40}$$

where $v_d$ is the velocity along the driving face of the blade ($\theta = 0$), which is determined from continuity considerations in the following paragraph.

Streamline distribution. - From continuity considerations and from the velocity distribution given by equation (40), the following expression is obtained for the streamline distribution (appendix F):

$$\psi = \frac{HR}{2\gamma RM_T}\left[\left\{1 + \frac{\gamma-1}{2}\left[(RM_T)^2 - \left(\frac{v_d}{c_o}\right)^2\right] - \frac{\Delta T_w}{T_o}\right\}^{\frac{\gamma}{\gamma-1}} - \left\{1 + \frac{\gamma-1}{2}\left[(RM_T)^2 - \left(\frac{v_d}{c_o} + 2RM_T\theta\right)^2\right] - \frac{\Delta T_w}{T_o}\right\}^{\frac{\gamma}{\gamma-1}}\right] \tag{41}$$

where the constant term $\Delta T_w/T_o$ is evaluated by equation (9a). The velocity ratio $v_d/c_o$ is obtained by equation (41) from the condition that

$$\psi = \psi_t = \varphi\sigma_T$$

when

$$\theta = \sigma$$

When the velocity ratio $v_d/c_o$ is determined, equation (41) expresses the streamline distribution as a function of the coordinates $R,\theta$ and the tip Mach number $M_T$.

Discussion. - The velocity ratio along the driving face of the blade $v_d/c_o$ has been computed from equation (41) for the same conditions used in the relaxation solution of this report. The results of this computation are shown in figure 16 and are compared with the results obtained from the relaxation solution. The agreement between the relaxation solution and the approximate solution is satisfactory up to a radius ratio of about 0.85. For radius ratios greater than 0.85, the assumption that the u component of the velocity, and its derivative, may be neglected is no longer valid because appreciable changes in the u component near the blade tip are required, from momentum considerations, to unload the blade.

In comparing the flow characteristics across the passage obtained from the relaxation solution and the approximate solution, the radius ratios 0.675 and 0.855 shown in figure 16 will be used.

The eddy formed on the driving face of the blade (fig. 10) has two stagnation points on the blade. The velocity along the driving face of the blade is zero at radius ratios corresponding to these stagnation points (fig. 13). The smaller radius ratio can be predicted by the approximate solution from the plot of $v_d/c_o$ in figure 16. The estimated value of the radius ratio is 0.703 compared with a value of 0.713 obtained by the relaxation solution. It therefore appears that the presence of the eddy can be predicted with fair accuracy provided the eddy occurs at a radius ratio for which the simplified analysis is valid, that is, for a radius ratio at which the u component of the velocity may be neglected.

The velocity distribution across the passage has been computed from equation (40) with the computed values of $v_d/c_o$ given in figure 16. This velocity distribution is plotted in figure 17 for

radius ratios of 0.675 and 0.855 and is compared with the corresponding velocity distribution obtained by the relaxation solution. The velocity distribution at a radius ratio of 0.675 is nearly the same for both solutions. At a radius ratio of 0.855, the agreement is still satisfactory although the slopes of the two curves have begun to deviate. This deviation between the solutions results from the blade unloading.

The streamline distribution across the passage has been computed from equation (41) with the computed values of $v_d/c_o$ given in figure 16. This streamline distribution is plotted in figure 18 for radius ratios of 0.675 and 0.855 and is compared with the corresponding streamline distribution obtained by the relaxation solution. The fact that the streamline distribution at a radius ratio of 0.675 is nearly the same for both solutions indicates that the boundary values of $\psi$ at the left bound $\psi_l$ (fig. 8) can be computed by the approximate method for radius ratios at least as high as approximately 0.65. At a radius ratio of 0.855, the streamline distribution, although satisfactory in a qualitative manner, has begun to deviate appreciably from the more rigorous relaxation solution.

Pressure ratio. - The pressure ratio in the impeller passage is given by (appendix F)

$$\frac{p}{p_o} = \left\{ 1 + \frac{\gamma-1}{2} \left[ (RM_T)^2 - \left( \frac{v_d}{c_o} + 2RM_T\theta \right)^2 \right] - \frac{\Delta T_w}{T_o} \right\}^{\frac{\gamma}{\gamma-1}} \qquad (42)$$

where $v_d/c_o$ is determined from continuity considerations as described on page 31.

The pressure ratio across the passage has been computed from equation (42) with the approximate values of $v_d/c_o$ given in figure 16. This pressure distribution is plotted in figure 19 for radius ratios of 0.675 and 0.855 and is compared with the corresponding pressure distribution obtained by the relaxation solution. The pressure distribution at a radius ratio of 0.675 is nearly the same for both solutions and at a radius ratio of 0.855 the agreement is satisfactory.

Blade loading. - The blade loading at any given conic-radius ratio is given by the difference in pressure between the driving face and the trailing face of the blade. From appendix F, this difference is given by

$$\frac{p_d - p_t}{p_o} = \frac{2\gamma RM_T}{HR}\varphi\sigma_T \tag{43}$$

The blade loading has been computed from equation (43) and is plotted in figure 20 together with the corresponding curve obtained from the relaxation solution. The two curves are in good agreement for radius ratios less than 0.825. At higher radius ratios, however, the blade unloads for the relaxation solution whereas the blade loading continues to increase for the approximate solution. In order to correct equation (43) for the blade unloading, the folflowing relation is assumed:

$$\frac{p_d - p_t}{p_o} = \frac{2\gamma RM_T}{HR}\varphi\sigma_T\,(1 - R^x) \tag{44}$$

where the exponent $x$ is determined by the slip factor $\mu$ from considerations given in appendix F

$$x = \frac{2\mu}{1 - \mu} \tag{45}$$

In the numerical example, the value of $\mu$ obtained from the relaxation solution is 0.90, for which, from equation (45), the value of $x$ is 18.0. Equation (44) for the blade loading therefore becomes

$$\frac{p_d - p_t}{p_o} = \frac{2\gamma RM_T}{HR}\varphi\sigma_T\,(1 - R^{18}) \tag{44a}$$

## CONCLUSIONS AND SUMMARY OF RESULTS

A general method of analysis has been developed for two-dimensional, steady, compressible flow in centrifugal compressors with arbitrary blade shapes, arbitrary variations in the passage height, and with fixed cone angles (right circular cones generated by the center line of the flow passage). From this analysis the following conclusions can be drawn:

The solution obtained for a given cone angle also applies to other cone angles (that is, other mixed-flow compressors) with a fewer or a greater number of passages but with the same included passage angle, and so forth. Mixed-flow compressors with the same number of flow passages as radial-discharge compressors and therefore with smaller included passage angles have lower peak blade loadings and lower maximum relative velocities than the corresponding radial-discharge compressors.

The general analysis also applies to inward-flow turbines. The solution obtained for a centrifugal compressor with smooth (shockless) entry is also the solution (with the flow direction and rotation reversed) for an inward-flow turnbine with the same design characteristics (that is, the same rotor) and with smooth (shockless) entry.

From a numerical example of a radial-discharge compressor with 20 straight blades lying on conic radii, constant flow area, an inlet radius ratio of zero, a tip Mach number of 1.5, and a flow coefficient of 0.5, the following results were obtained:

1. A wheel-type eddy formed on the driving face of the impeller.

2. The velocities and pressures at the impeller tip were reasonably uniform and any nonuniformity in the flow leaving the impeller rapidly adjusted itself.

3. The maximum local Mach number relative to the impeller was 0.64 and occurred along the trailing face of the blade at 68 percent of the tip radius.

4. The computed slip factor was 0.90.

In addition, a simplified analysis for straight blades lying on conic radii is presented which can be used to determine the streamlines, pressure distribution, and velocity profiles within the impeller except near the tip (and inlet).

Lewis Flight Propulsion Laboratory,
National Advisory Committee for Aeronautics,
Cleveland, Ohio, August 18, 1948.

## APPENDIX A

## SYMBOLS

The following symbols are used in the analysis:



| | |
|---|---|
| A | flow-area ratio, $a/a_T$ |
| a | flow area, normal to conic surface |
| B | number of blades (or passages) |
| b | grid spacing (fig. 3) |
| c | local speed of sound |
| $c_p$ | specific heat at constant pressure |
| F | any twice-differentiable function of two variables |
| g | acceleration due to gravity |
| H | passage-height ratio, $h/h_T$ |
| h | passage height, normal to conic surface |
| J | mechanical equivalent of heat |
| K | constant |
| $M_T$ | impeller tip Mach number, $\frac{\omega r_T \sin \frac{\alpha}{2}}{c_o}$ |
| m | passage-height exponent |
| N | constant |
| p | static pressure |
| Q | residual |
| q | velocity relative to impeller, $\sqrt{u^2 + v^2}$ |
| R | conic-radius ratio, $r/r_T$ |
| r | conic radius (distance along conic element from apex of cone) |
| T | absolute temperature |

$u$ tangential component of velocity relative to impeller (positive in direction of rotation)

$v$ radial (along conic element) component of velocity

$W$ compressor flow rate (total)

$w$ flow rate between streamlines

$x$ exponent for blade-loading correction

$z$ complex variable

$\alpha$ cone angle (fig. 1)

$\beta$ blade curvature angle (fig. 6)

$\Gamma$ absolute circulation

$\gamma$ ratio of specific heats

$\Delta$ finite increment

$\delta$ ratio of inlet stagnation pressure to standard sea-level pressure

$\eta$ transformed coordinate (incompressible stream function)

$\theta$ angle, radians (fig. 2)

$\theta$ ratio of inlet stagnation temperature to standard sea-level temperature

$\mu$ slip factor

$\xi$ transformed coordinate (incompressible velocity potential)

$\rho$ weight density of fluid

$\sigma$ included passage angle, $(\theta_t - \theta_d)$

$\tau$ impeller torque

$\varphi$ flow coefficient, $\frac{W}{\rho_o a_T c_o}$

$\psi$ compressible stream function

$\omega$ impeller angular velocity

Subscripts:

| | |
|---|---|
| av | average |
| d | driving face of blade (fig. 8) |
| e | upper bound of diffuser (fig. 8) |
| f | lower bound of diffuser (fig. 8) |
| I | impeller inlet |
| i | incompressible flow |
| l | left bound (fig. 8) |
| o | absolute inlet stagnation condition |
| r | right bound (fig. 8) |
| S | simplified solution |
| T | impeller tip |
| t | trailing face of blade (fig. 8) |
| w | whirl ahead of impeller |
| R, $\theta$, $\xi$, and $\eta$ | partial derivatives with respect to R, $\theta$, $\xi$, and $\eta$, respectively |
| RR, $\theta\theta$, R$\theta$, $\xi\xi$, $\eta\eta$, and $\xi\eta$ | second partials with respect to R, $\theta$, R and $\theta$, $\xi$, $\eta$, and $\xi$ and $\eta$, respectively |
| 1, 2, 3, and 4 | grid points adjacent to point in question (fig. 3) |

## APPENDIX B

## TRANSFORMATION OF GENERAL DIFFERENTIAL EQUATION FOR FLOW IN CENTRIFUGAL COMPRESSOR FROM R,$\theta$ TO $\xi$,$\eta$ COORDINATES

The conformal transformation (except for singular points) from the R$\theta$- to the $\xi\eta$-plane, where $\xi$ and $\eta$ are the velocity potential and stream function, respectively, for incompressible flow through the stationary impeller ($\omega = 0$) with constant passage height ($H = 1$), is given by the analytic function

$$f(z) = f(Re^{i\theta}) = \xi\,(R,\theta) + i\eta\,(R,\theta) \tag{13}$$

where $\xi$ and $\eta$ are functions of R and $\theta$. Therefore,

$$\left.\begin{aligned} F_R &= F_\xi\,\xi_R + F_\eta\,\eta_R \\ F_{RR} &= F_{\xi\xi}\,\xi_R^2 + 2F_{\xi\eta}\,\xi_R\,\eta_R + F_{\eta\eta}\,\eta_R^2 + F_\xi\,\xi_{RR} + F_\eta\,\eta_{RR} \\ F_\theta &= F_\xi\,\xi_\theta + F_\eta\,\eta_\theta \\ F_{\theta\theta} &= F_{\xi\xi}\,\xi_\theta^2 + 2F_{\xi\eta}\,\xi_\theta\,\eta_\theta + F_{\eta\eta}\,\eta_\theta^2 + F_\xi\,\xi_{\theta\theta} + F_\eta\,\eta_{\theta\theta} \end{aligned}\right\} \tag{46}$$

The velocity potential $\xi$ and the stream function $\eta$ are related by the Cauchy-Riemann differential equations

$$\left.\begin{aligned} v_1 &= \xi_R = \frac{\eta_\theta}{R} \\ u_1 &= \frac{\xi_\theta}{R} = -\eta_R \end{aligned}\right\} \tag{47}$$

After equations (46) and (47) are combined, the first three terms of the right side of equation (6) become

$$\psi_{RR} + \frac{\psi_R}{R} + \frac{\psi_{\theta\theta}}{R^2} = \left(\psi_{\xi\xi} + \psi_{\eta\eta}\right)\left(\frac{\eta_\theta^2}{R^2} + \eta_R^2\right) + \psi_\eta \left(\eta_{RR} + \frac{\eta_R}{R} + \frac{\eta_{\theta\theta}}{R^2}\right)$$

But, because $f(z)$ is analytic,

$$\eta_{RR} + \frac{\eta_R}{R} + \frac{\eta_{\theta\theta}}{R^2} = 0$$

and from equation (47),

$$\frac{\eta_\theta^2}{R^2} + \eta_R^2 = v_i^2 + u_i^2 = q_i^2$$

where $q_i$ is the velocity for incompressible flow through the stationary impeller ($\omega = 0$) with constant blade height ($H = 1$). Therefore,

$$\psi_{RR} + \frac{\psi_R}{R} + \frac{\psi_{\theta\theta}}{R^2} = q_i^2 \left(\psi_{\xi\xi} + \psi_{\eta\eta}\right) \tag{48}$$

The fourth term of the right side of equation (6) becomes

$$\begin{aligned}\psi_R (\log_e H)_R &= \left(\psi_\xi \frac{\eta_\theta}{R} + \psi_\eta \eta_R\right)\left[(\log_e H)_\xi \frac{\eta_\theta}{R} + (\log_e H)_\eta \eta_R\right] \\ &= \left(\psi_\xi v_i - \psi_\eta u_i\right)\left[(\log_e H)_\xi v_i - (\log_e H)_\eta u_i\right]\end{aligned} \tag{49}$$

where $H$ is now a function of $\xi$ and $\eta$ instead of $R$ alone.

The last two terms of equation (6) in like manner become

$$\psi_R\left(\log_e \frac{\rho}{\rho_o}\right)_R + \frac{\psi_\theta}{R^2}\left(\log_e \frac{\rho}{\rho_o}\right)_\theta = \left[\psi_\xi\left(\log_e \frac{\rho}{\rho_o}\right)_\xi + \psi_\eta\left(\log_e \frac{\rho}{\rho_o}\right)_\eta\right]\left(\frac{\eta_\theta^2}{R^2} + \eta_R^2\right)$$

$$= q_1^2\left[\psi_\xi\left(\log_e \frac{\rho}{\rho_o}\right)_\xi + \psi_\eta\left(\log_e \frac{\rho}{\rho_o}\right)_\eta\right] \tag{50}$$

After combining equations (48) to (50), equation (6) becomes

$$\frac{2M_T^2}{q_1^2}\frac{\rho}{\rho_o}H = \psi_{\xi\xi} + \psi_{\eta\eta} - \psi_\xi\left(\log_e \frac{\rho}{\rho_o}\right)_\xi - \psi_\eta\left(\log_e \frac{\rho}{\rho_o}\right)_\eta$$

$$- \frac{1}{q_1^2}\left(\psi_\xi v_1 - \psi_\eta u_1\right)\left[\left(\log_e H\right)_\xi v_1 - \left(\log_e H\right)_\eta u_1\right] \tag{14}$$

## APPENDIX C

## DIFFERENTIAL EQUATION FOR FLOW THROUGH CENTRIFUGAL COMPRESSORS WITH LOGARITHMIC-SPIRAL BLADES

Consider the analytic function,

$$\begin{aligned} f(z) &= (N + iK) \log_e z \\ &= (N + iK) \log_e (Re^{i\theta}) \\ &= (N + iK) (\log_e R + i\theta) \\ &= (N \log_e R - K\theta) + i(K \log_e R + N\theta) \end{aligned} \tag{28}$$

where $N$ and $K$ are constants to be determined by the boundary conditions. From equations (13) and (28),

$$\xi = N(\log_e R - \frac{K}{N} \theta) \tag{29}$$

and

$$\eta = N(\frac{K}{N} \log_e R + \theta) \tag{29a}$$

The blade shape in the $R\theta$-plane is given by equation (29a), which, with $\eta$ constant, determines a logarithmic spiral (fig. 6).

In order to determine the constants $N$ and $K$, equation (29a) is differentiated with $\eta$ constant,

$$0 = \frac{K}{N} \frac{dR}{R} + d\theta$$

or

$$\frac{K}{N} = - \frac{R d\theta}{dR}$$

But, from figure 6

$$\beta = \tan^{-1} \frac{R d\theta}{dR}$$

1015

where $\beta$ is the angle between blade surface and conic-radius ratio R on R$\theta$-plane (and on conic surface). Therefore,

$$\frac{K}{N} = - \tan \beta = \text{constant}$$

and equation (29a) becomes

$$\eta = N(\theta - \tan \beta \log_e R) \tag{51}$$

In order to determine the constant N, let

$$\eta = \psi_t$$

when

$$\theta = \sigma_T$$

and

$$R = 1.0$$

(from which the zero point for $\theta$ is at the tip of the driving face of the blade). Therefore, from equation (51),

$$N = \frac{\psi_t}{\sigma_T}$$

which, from equation (25), is equal to the flow coefficient $\varphi$ and the final expressions for $\xi$ and $\eta$ become

$$\xi = \varphi(\log_e R + \theta \tan \beta) \tag{30}$$

$$\eta = \varphi(\theta - \tan \beta \log_e R) \tag{30a}$$

These equations relate points in the R$\theta$-plane to corresponding points in the $\xi\eta$-plane. Solving equations (30) and (30a) for R and $\theta$ in terms of $\xi$ and $\eta$ gives

$$R = e^{\frac{\xi - \eta \tan \beta}{\varphi \sec^2 \beta}} \tag{31}$$

$$\theta = \frac{\eta + \xi \tan \beta}{\varphi \sec^2 \beta} \tag{31a}$$



From equations (15), (30a), and (31),

$$u_1 = \varphi \tan \beta \, e^{\frac{\eta \tan \beta - \xi}{\varphi \sec^2 \beta}} \tag{52}$$

and

$$v_1 = \varphi e^{\frac{\eta \tan \beta - \xi}{\varphi \sec^2 \beta}} \tag{52a}$$

so that

$$q_1 = \sqrt{u_1^2 + v_1^2} \tag{10}$$

$$= \varphi \sec \beta \, e^{\frac{\eta \tan \beta - \xi}{\varphi \sec^2 \beta}} \tag{52b}$$

From equations (14) and (52) to (52b), the differential equation for the flow of compressible fluid through centrifugal compressors with logarithmic-spiral blades becomes, in terms of the transformed coordinates $\xi$ and $\eta$,

$$2M_T \frac{\rho}{\rho_o} H \frac{e^{\frac{2(\xi - \eta \tan \beta)}{\varphi \sec^2 \beta}}}{(\varphi \sec \beta)^2} = \psi_{\xi\xi} + \psi_{\eta\eta} - \psi_\xi \left(\log_e \frac{\rho}{\rho_o}\right)_\xi - \psi_\eta \left(\log_e \frac{\rho}{\rho_o}\right)_\eta$$

$$- (\psi_\xi \cos \beta - \psi_\eta \sin \beta) \left[ (\log_e H)_\xi \cos \beta - (\log_e H)_\eta \sin \beta \right] \tag{32}$$

## APPENDIX D

## PROCEDURE FOR ESTIMATING BOUNDARY VALUES OF STREAM FUNCTION $\psi$ IN VANELESS DIFFUSERS

Estimated boundary values of the stream function $\psi$ in vaneless diffusers can be obtained by assuming, as a first approximation, that the flow in vaneless diffusers is one dimensional, that is, a function of R only. From the conservation of the moment of momentum,

$$r \sin \frac{\alpha}{2}\left(\omega r \sin \frac{\alpha}{2} + u\right) = r_T \sin \frac{\alpha}{2}\left(\mu \omega r_T \sin \frac{\alpha}{2}\right)$$

where $\mu$, the slip factor, is defined in appendix E. Therefore, solving for $u$, dividing by $c_o$, and expressing in terms of R

$$\frac{u}{c_o} = M_T\left(\frac{\mu}{R} - R\right) \tag{53}$$

In general, the slip factor $\mu$ depends upon the blade shape and upon the operating conditions of the compressor. Combining equations (4a) and (53) gives

$$\psi_R = \frac{\rho H M_T}{\rho_o}\left(R - \frac{\mu}{R}\right) \tag{54}$$

This equation gives the variation in the stream function with the radius ratio R for a constant value of $\theta$. Because the density ratio is also a function of R, equation (54) is solved by numerical point-by-point methods. In order to obtain this solution, it is first necessary to know the density variation with R.

The density ratio is given by

$$\frac{\rho}{\rho_o} = 1 + \frac{\gamma-1}{2}\left[\left(RM_T\right)^2 - \left(\frac{q}{c_o}\right)^2 - \frac{\Delta T_w}{T_o}\right]^{\frac{1}{\gamma-1}} \tag{11}$$

where

$$\left(\frac{q}{c_o}\right)^2 = \left(\frac{u}{c_o}\right)^2 + \left(\frac{v}{c_o}\right)^2$$

which, from equations (26) and (53) and from continuity considerations, assuming $a_T = 2\pi \sin\frac{\alpha}{2} h_T r_T$,

$$\left(\frac{q}{c_o}\right)^2 = M_T^2 \left(\frac{\mu}{R} - R\right)^2 + \left(\frac{\varphi}{\frac{\rho}{\rho_o} HR}\right)^2$$

so that the density ratio becomes

$$\frac{\rho}{\rho_o} = \left\{1 + \frac{\gamma-1}{2} M_T^2 \left[2\mu - \frac{\mu}{R}^2 - \left(\frac{\varphi}{\frac{\rho}{\rho_o} HRM_T}\right)^2\right]\right\}^{\frac{1}{\gamma-1}} \qquad (55)$$

The upper or lower boundary values of the diffuser $\psi_e$ or $\psi_f$ (fig. 8) are therefore estimated from equations (54) and (55) using assumed values of the slip factor. These estimated boundary values are not generally the correct values and provision must be made in the relaxation solution for their correction in the same manner that any other estimated values of $\psi$ are corrected.

## APPENDIX E

## PROCEDURE FOR COMPUTING IMPELLER SLIP FACTOR

The impeller slip factor is defined as the ratio of the average absolute tangential velocity of the air as it leaves the impeller tip to the tip speed of the impeller.

$$\text{slip factor} = \mu = \frac{\left(\omega r_T \sin\frac{\alpha}{2} + u\right)_{av}}{\omega r_T \sin\frac{\alpha}{2}} = 1 + \frac{u_{av}}{\omega r_T \sin\frac{\alpha}{2}}$$

$$= 1 + \frac{\left(\frac{u}{c_o}\right)_{av}}{M_T} \tag{56}$$

The average value of the tangential velocity relative to the impeller at the impeller tip is given by

$$\left(\frac{u}{c_o}\right)_{av} = \frac{\int_{\theta_d}^{\theta_t} \left(\frac{u}{c_o}\right) \rho v h_T r_T \, d\theta}{\int_{\theta_d}^{\theta_t} \rho v h_T r_T \, d\theta}$$

$$= \frac{\rho_o c_o h_T r_T}{\frac{W}{B}} \int_{\theta_d}^{\theta_t} \left(\frac{u}{c_o}\right)\left(\frac{\rho}{\rho_o}\right)\left(\frac{v}{c_o}\right) d\theta$$

which, from equations (22) and (25), reduces to

$$\left(\frac{u}{c_o}\right)_{av} = \frac{1}{\varphi} \int_0^1 \left(\frac{u}{c_o}\right)\left(\frac{\rho}{\rho_o}\right)\left(\frac{v}{c_o}\right) d\left(\frac{\theta - \theta_d}{\sigma_T}\right) \tag{57}$$

Equation (58) gives a weighted average value of $u/c_o$. This weighted average value of $u/c_o$ is also equal to the unweighted average value of $u/c_o$, which is equal to $\frac{1}{\sigma_T}\int_{\theta_d}^{\theta_t}\left(\frac{u}{c_o}\right)d\theta$. This fact can be shown from considerations of the conservation of angular momentum in the diffuser, which is based upon the weighted average value of $u/c_o$ and from considerations of constant absolute circulation in the diffuser, which is based upon the unweighted average value of $u/c_o$. Combining equations (56) and (57) results in the following expression for the slip factor:

$$\mu = 1 + \frac{1}{\varphi M_T}\int_0^1 \left(\frac{u}{c_o}\right)\left(\frac{\rho}{\rho_o}\right)\left(\frac{v}{c_o}\right) d\left(\frac{\theta - \theta_d}{\sigma_T}\right) \qquad (58)$$

The value of the integral is obtained from the area under a curve of the integrand evaluated at the impeller tip as a function of the angle ratio $\frac{\theta - \theta_d}{\sigma_T}$ (fig. 21). The value of the integrand is obtained from the relaxation solution.

## APPENDIX F

## SIMPLIFIED ANALYSIS FOR RADIAL-DISCHARGE AND MIXED-FLOW CENTRIFUGAL COMPRESSORS WITH STRAIGHT BLADES ALONG CONIC RADII

Velocity distribution. - This simplified analysis is based on the assumption that for centrifugal compressors with straight blades along conic radii the tangential component of the velocity relative to the impeller is zero at all radii within the impeller. The irrotationality equation (5) therefore reduces to

$$2\omega r_T \sin\frac{\alpha}{2} = \frac{1}{R}\frac{\partial v}{\partial \theta}$$

which, when integrated with respect to $\theta$ between limits, becomes

$$v = v_d + 2\omega r_T \sin\frac{\alpha}{2} R\theta$$

which, in turn, divided by the speed of sound at inlet stagnation conditions becomes

$$\frac{v}{c_o} = \frac{v_d}{c_o} + 2RM_T\,\theta \qquad (40)$$

where $v_d$ is determined from continuity considerations in the following paragraph.

Streamline distribution. - Neglecting the u component of velocity, the continuity equation becomes (fig. 2):

$$dw = \rho v h_T r_T H R d\theta$$

The density $\rho$ is obtained from equation (11) with $q/c_o$ equal to $v/c_o$ and the velocity ratio $v/c_o$ is obtained from equation (40), so that

$$\frac{dw}{\rho_o c_o h_T r_T} = HR \left\{ 1 + \frac{\gamma-1}{2} \left[ (RM_T)^2 - \left( \frac{v_d}{c_o} + 2RM_T\theta \right)^2 \right] - \frac{\Delta T_w}{T_o} \right\}^{\frac{1}{\gamma-1}} \left( \frac{v_d}{c_o} + 2RM_T\theta \right) d\theta \qquad (59)$$

where the constant term $\Delta T_w/T_o$ is evaluated by equation (9a). Integrating the right side of equation (59) between the limits 0 and $\theta$ and noting from equation (20) that the left side of equation (59) is equal to $d\psi$, which is integrated between 0 and $\psi$, gives

$$\psi = \frac{HR}{2\gamma RM_T} \left[ \left\{ 1 + \frac{\gamma-1}{2} \left[ (RM_T)^2 - \left( \frac{v_d}{c_o} \right)^2 \right] - \frac{\Delta T_w}{T_o} \right\}^{\frac{\gamma}{\gamma-1}} - \left\{ 1 + \frac{\gamma-1}{2} \left[ (RM_T)^2 - \left( \frac{v_d}{c_o} + 2RM_T\theta \right)^2 \right] - \frac{\Delta T_w}{T_o} \right\}^{\frac{\gamma}{\gamma-1}} \right] \qquad (41)$$

Equation (41) expresses the streamline distribution as a function of the coordinates $R,\theta$ and the tip Mach number $M_T$. The velocity ratio $v_d/c_o$ is obtained by equation (41) from the condition that

$$\psi = \psi_t = \varphi\sigma_T$$

when

$$\theta = \sigma$$

Pressure ratio. - The pressure ratio is directly determined from the temperature ratio by the thermodynamic relation

$$\frac{p}{p_o} = \left( \frac{T}{T_o} \right)^{\frac{\gamma}{\gamma-1}}$$

The temperature ratio is given by equation (9) in which the velocity ratio $q/c_o$ is equal to $v/c_o$ given by equation (40) so that

$$\frac{p}{p_o} = \left\{1 + \frac{\gamma-1}{2}\left[(RM_T)^2 - \left(\frac{v_d}{c_o} + 2RM_T\theta\right)^2\right] - \frac{\Delta T_w}{T_o}\right\}^{\frac{\gamma}{\gamma-1}} \tag{42}$$

where $v_d/c_o$ is determined from continuity considerations as previously described.

Substituting equation (42) into equation (41) results in

$$\psi = \frac{HR}{2\gamma RM_T}\left(\frac{p_d}{p_o} - \frac{p}{p_o}\right) \tag{60}$$

The stream function $\psi$ and the pressure ratio $p/p_o$ are therefore related by the simple equation (60).

Blade loading. - The blade loading at any given radius ratio is given by the difference in pressure between the driving and trailing faces of the blade. From equation (60) this difference is

$$\frac{p_d - p_t}{p_o} = \frac{2\gamma RM_T}{HR}\,\psi_t$$

which, from equation (25), becomes

$$\frac{p_d - p_t}{p_o} = \frac{2\gamma RM_T}{HR}\,\varphi\sigma_T \tag{43}$$

The blade loading has been computed from equation (43) and is plotted against the conic-radius ratio R in figure 20 together with the corresponding curve obtained from the relaxation solution. The two curves are in good agreement for radius ratios less than 0.825. At higher radius ratios, however, the blade unloads for the relaxation solution, whereas the blade loading continues to increase for the approximate solution. In order to correct equation (43) for the blade unloading, the following relation is assumed,

$$\frac{p_d - p_t}{p_o} = \frac{2\gamma R M_T}{HR} \varphi\sigma_T (1 - R^x) \tag{44}$$

where the exponent $x$ is determined by the slip factor from the following considerations:

The impeller torque $\tau$ is obtained from the differential equation

$$d\tau = Bp_o \left(\frac{p_d - p_t}{p_o}\right) hr \sin\frac{\alpha}{2}\, dr$$

which expressed in terms of the dimensionless coordinates $H$ and $R$ and combined with equation (44) results in

$$d\tau = Bp_o\, 2\gamma M_T\, \varphi\sigma_T h_T r_T^2 \sin\frac{\alpha}{2} R(1 - R^x)\, dR$$

Integrating between the limits of $R$ equal to 0, assuming the blades extend to the origin, and $R$ equal to 1.0 gives

$$\tau = Bp_o\, \gamma M_T \varphi\sigma_T h_T r_T^2 \sin\frac{\alpha}{2} \left(\frac{x}{x+2}\right) \tag{61}$$

The torque can also be obtained from an expression for the impeller power, which includes the slip factor $\mu$,

$$\omega\tau = \frac{\mu}{g} \left(\omega r_T \sin\frac{\alpha}{2}\right)^2 W$$

which, after having been combined with equations (7), (23), and (26), the terms being rearranged, becomes

$$\tau = Bp_o\, \gamma M_T \varphi\sigma_T h_T r_T^2 \sin\frac{\alpha}{2} (\mu) \tag{62}$$

From equations (61) and (62), the exponent $x$ is obtained as a function of the slip factor $\mu$.

$$x = \frac{2\mu}{1 - \mu} \tag{45}$$

1015

The value of $\mu$ obtained from the relaxation solution is 0.90 $r$ which, from equation (45), the value of $x$ is 18.0. Equation (44) for the blade loading therefore becomes

$$\frac{p_d - p_t}{p_o} = \frac{2\gamma RM_T}{HR}\varphi\sigma_T\,(1 - R^{18}) \qquad (44a)$$

1015

## REFERENCES


1. Stodola, A.: Steam and Gas Turbines. Vol. II. McGraw-Hill Book Co., Inc., 6th ed., 1927, pp. 998-1006, 1255-1260.

2. Sörensen, E.: Potential Flow through Centrifugal Pumps and Turbines. NACA TM No. 973, 1941.

3. Betz, A., and Flügge-Lotz, I.: Design of Centrifugal Impeller Blades. NACA TM No. 902, 1939.

4. Bollay, William: The Theory of Flow through Centrifugal Pumps. Theodore von Kármán Anniversary Vol., Contributions to Appl. Mech. and Related Subjects, C.I.T., May 11, 1941, pp. 273-284.

5. Concordia, C., and Carter, G. K.: D-C Network-Analyzer Determination of Fluid-Flow Pattern in a Centrifugal Impeller. Jour. Appl. Mech., vol. 14, no. 2, June 1947, pp. A113-A118.

6. Southwell, R. V.: Relaxation Methods in Engineering Science. Clarendon Press (Oxford), 1940.

7. Southwell, R. V.: Relaxation Methods in Theoretical Physics. Clarendon Press (Oxford), 1946.

8. Emmons, Howard W.: The Numerical Solution of Compressible Fluid Flow Problems. NACA TN No. 932, 1944.

9. NACA Subcommittee on Compressors: Standard Procedures for Rating and Testing Multistage Axial-Flow Compressors. NACA TN No. 1138, 1946.

10. Emmons, Howard W.: The Numerical Solution of Partial Differential Equations. Quarterly Appl. Math., vol. II, no. 3, Oct. 1944, pp. 173-195.

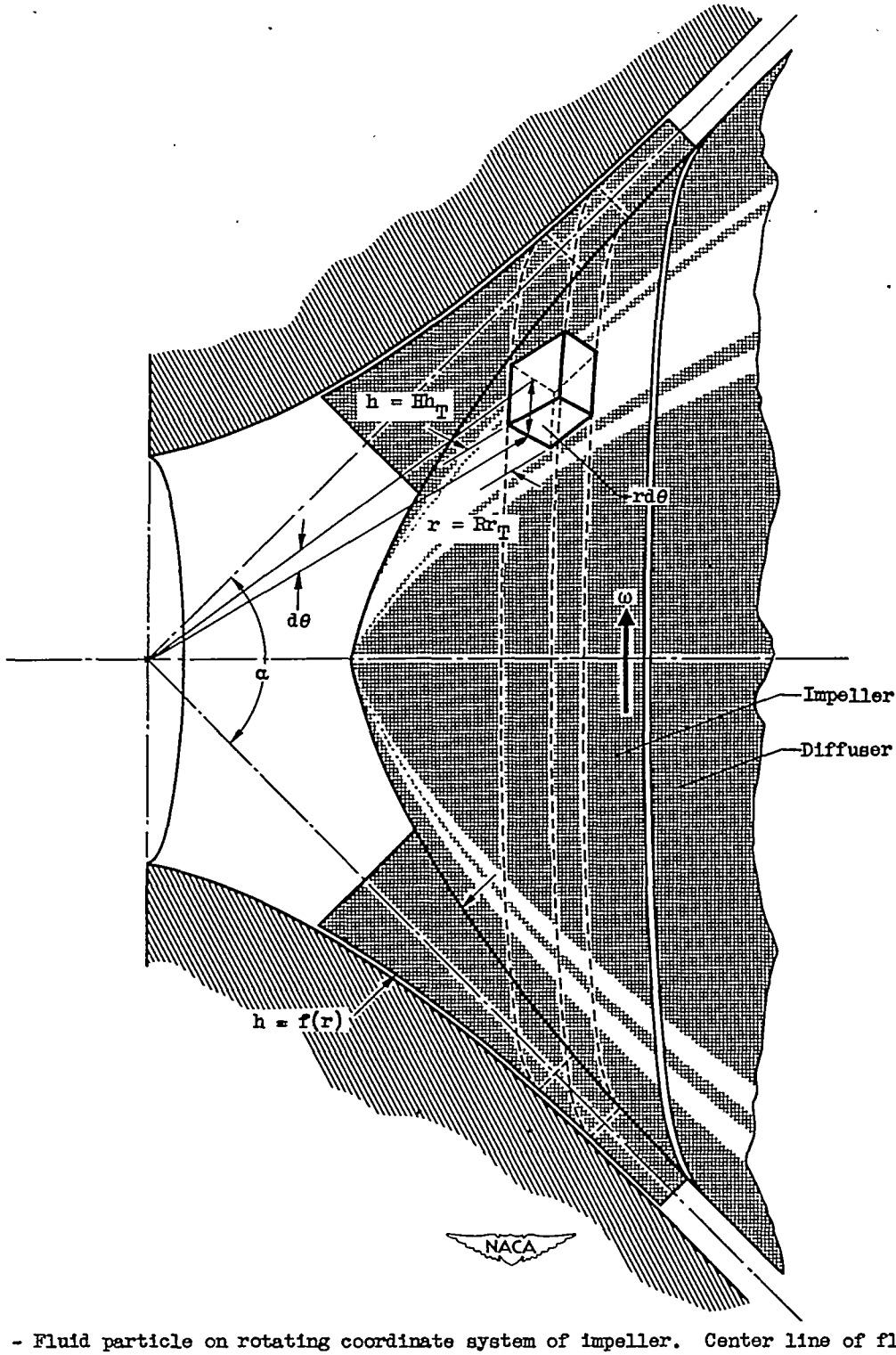


Figure 1. - Fluid particle on rotating coordinate system of impeller. Center line of flow passage generates right circular cone with cone angle α.

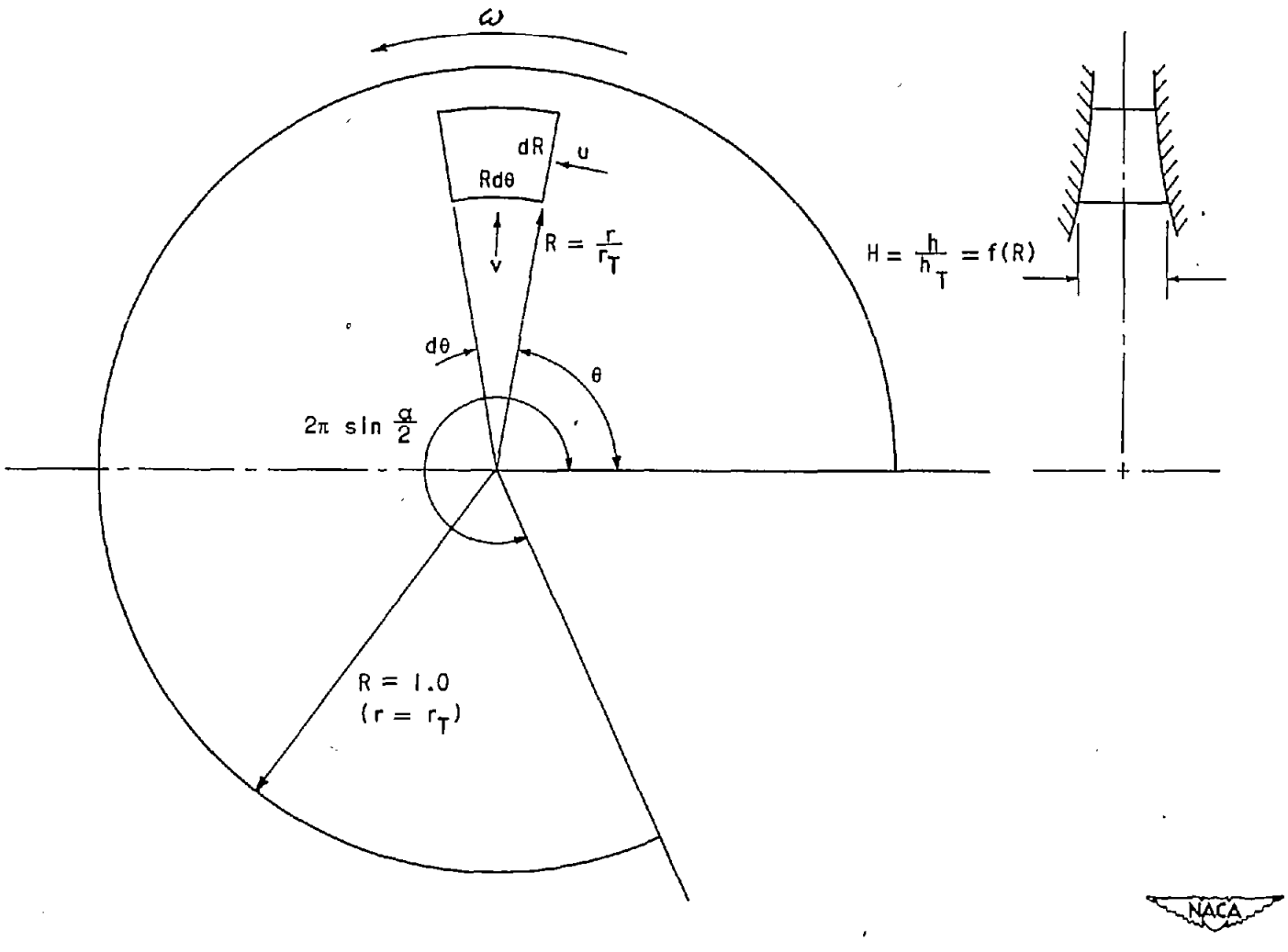


Figure 2. - Fluid particle on developed view of conic surface. R, θ, and H, dimensionless coordinates relative to impeller; u and v, tangential and radial components of velocity relative to impeller, respectively.

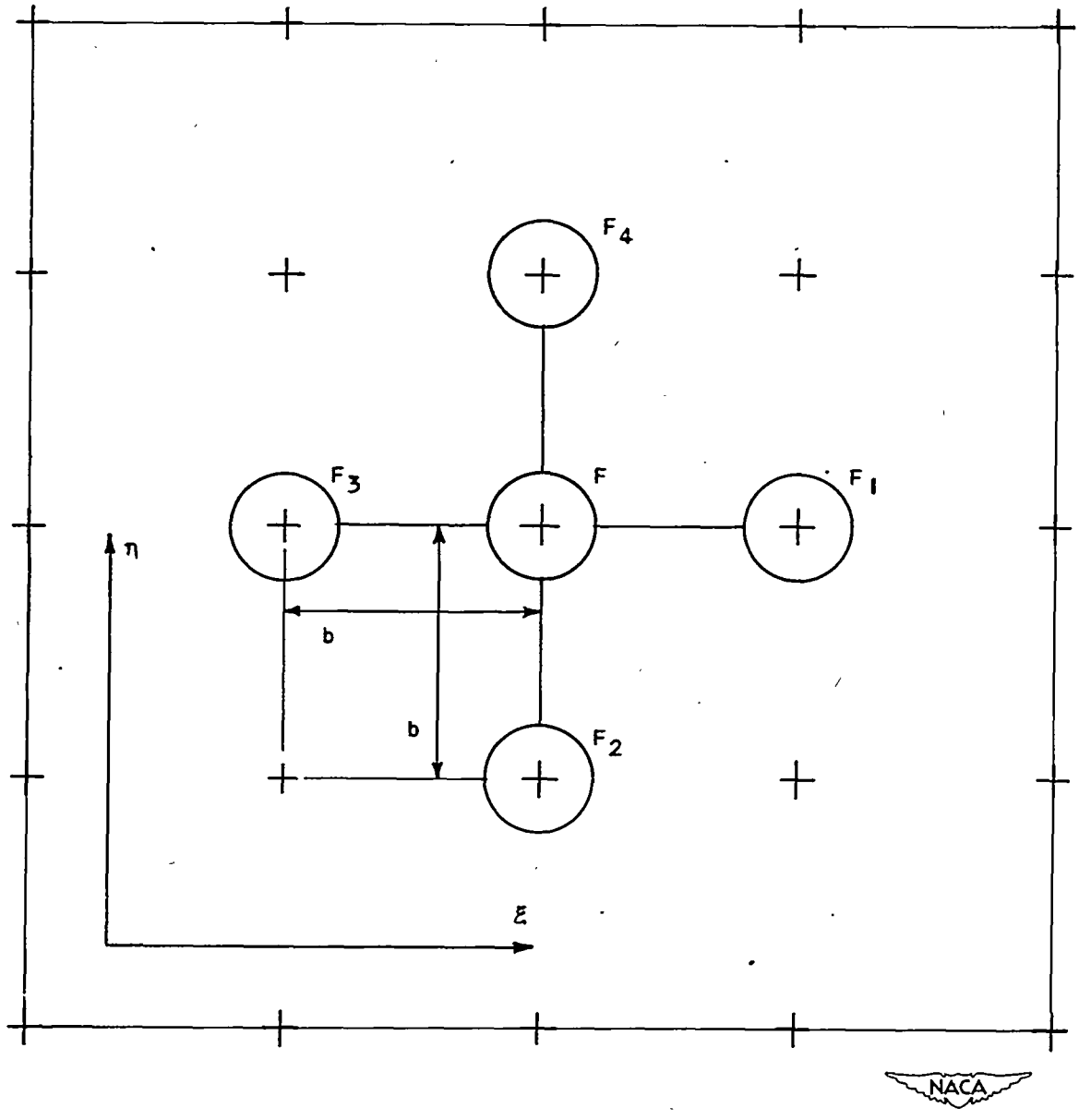


Figure 3. - Sample grid showing grid spacing b and numerical subscript convention for adjacent grid points.

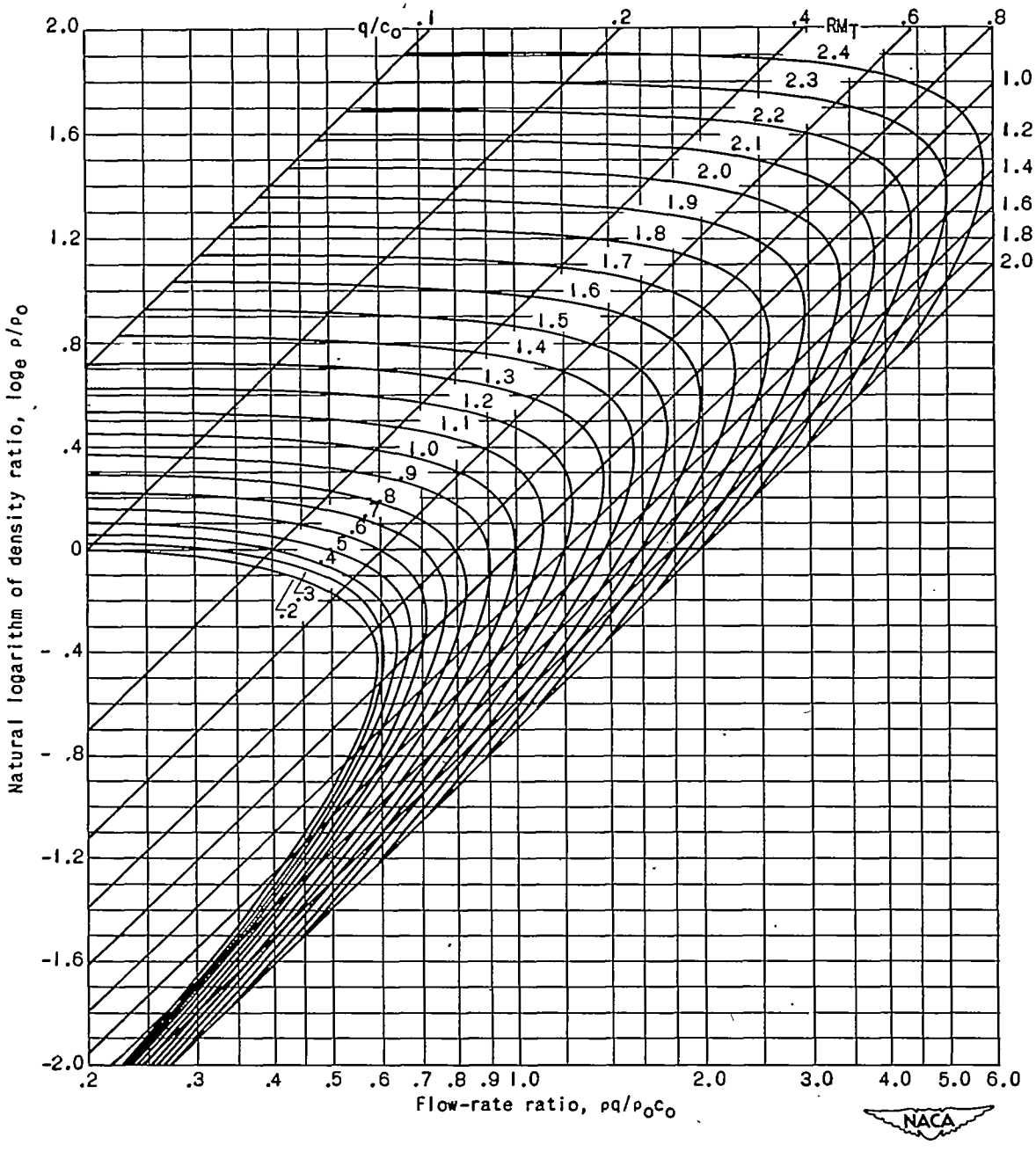


Figure 4. - Natural logarithm of density ratio $\log_e \rho/\rho_o$ as function of flow-rate ratio $\rho q/\rho_o c_o$ for various values of $RM_T$. Equation (11), ratio of specific heats equal to 1.4; whirl ahead of impeller equal to zero.

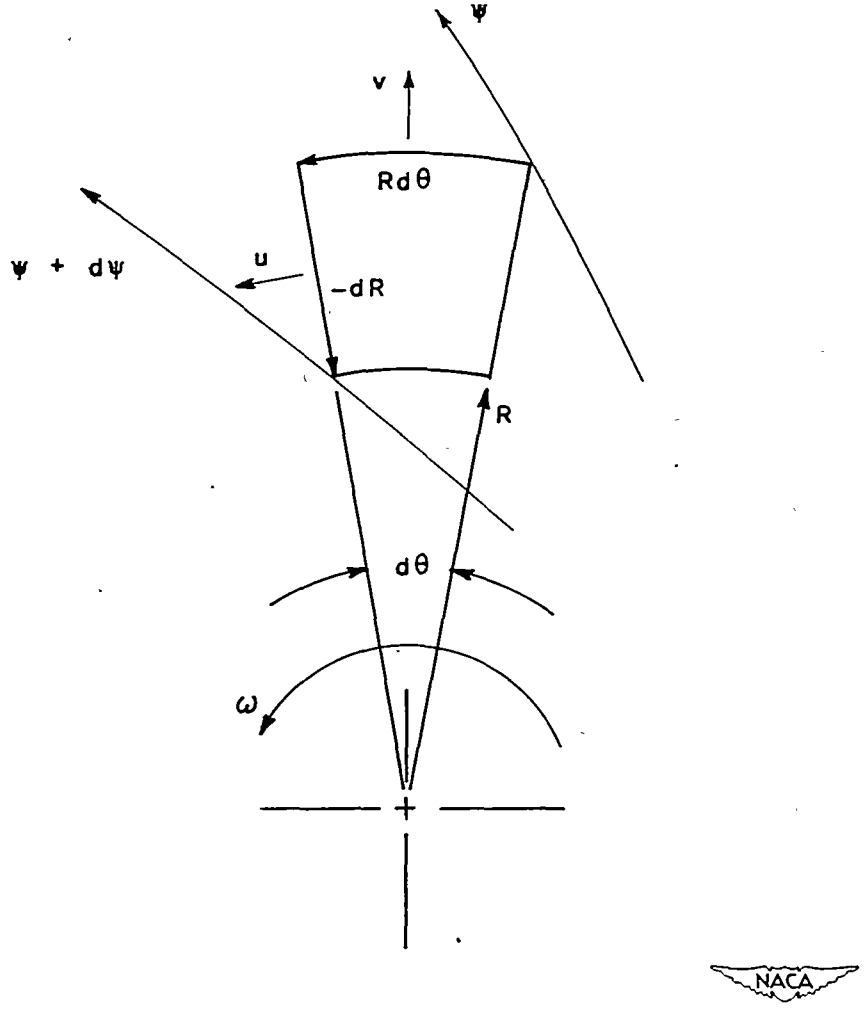


Figure 5. - Fluid particle between adjacent streamlines. Radial component of flow rate, $\rho v h_T r_T H R d\theta$; tangential component of flow rate, $-\rho u h_T r_T H dR$.

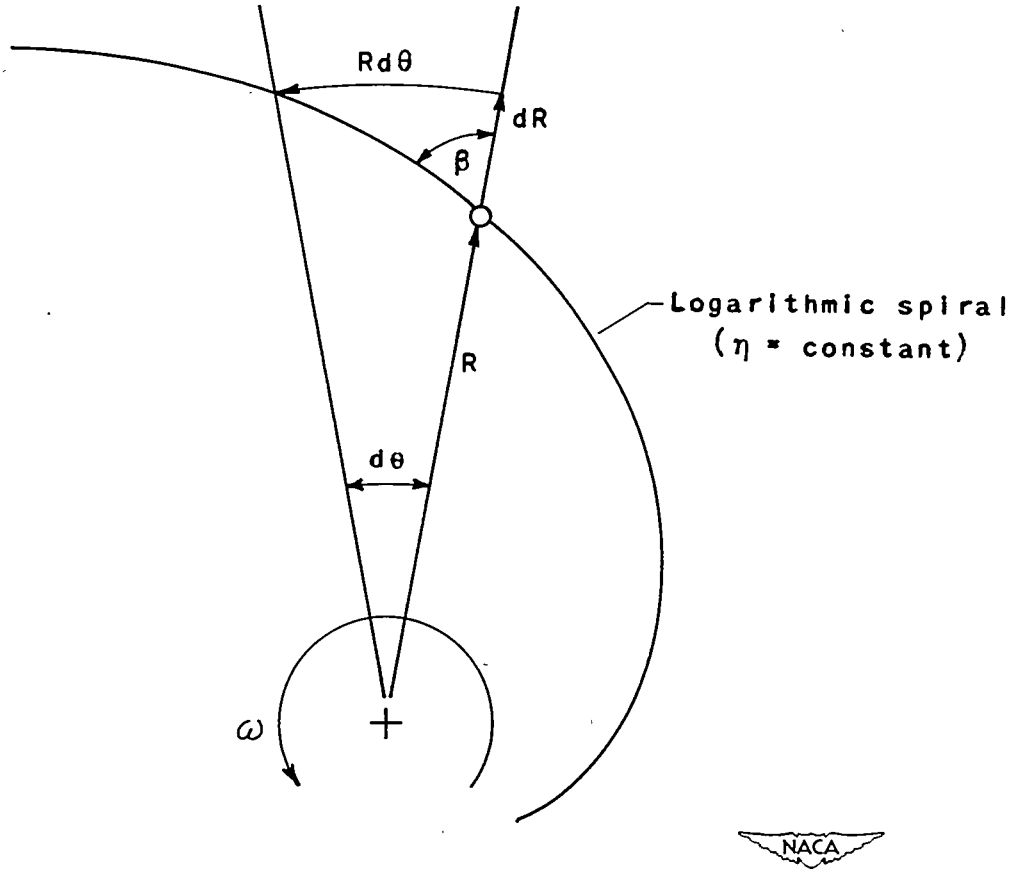


Figure 6. – Logarithmic-spiral blade shape.

Backward-curved blade, $\beta < 0$
Straight radial blade, $\beta = 0$
Forward-curved blade, $\beta > 0$

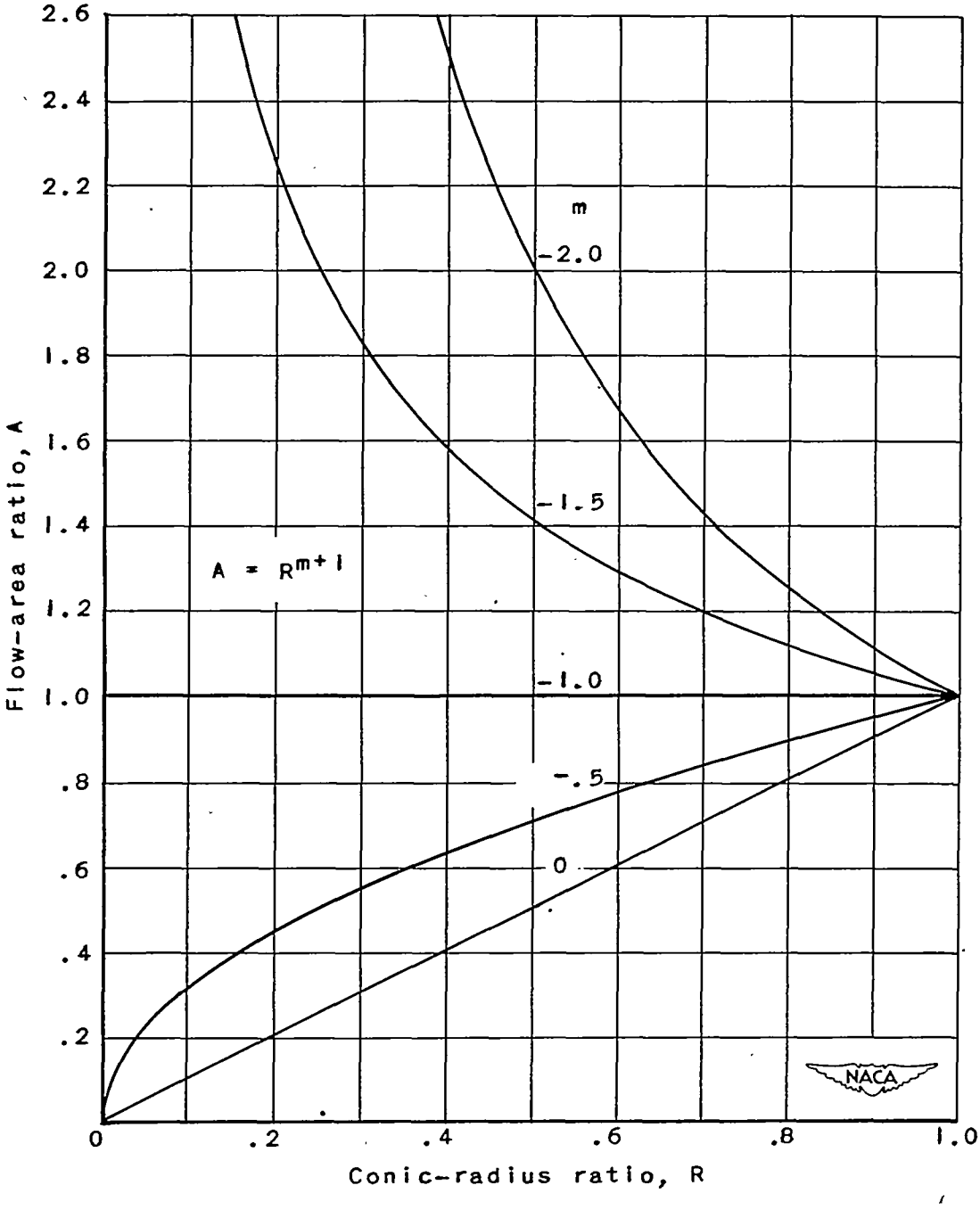


Figure 7. - Flow-area-ratio variation with conic-radius ratio for several values of exponent m. Blade thickness assumed to be a constant percentage of passage width at all conic-radius ratios.

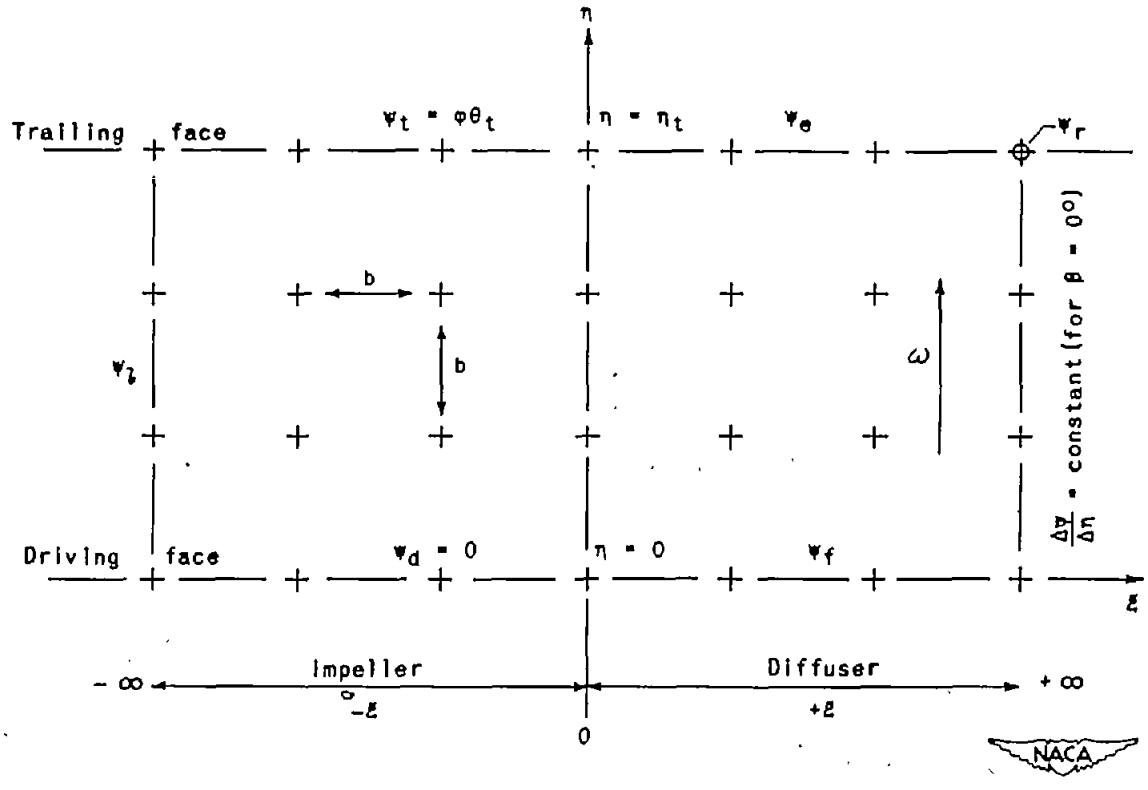


Figure 8. - Relaxation grid in transformed coordinates showing boundary values of ψ discussed in text.

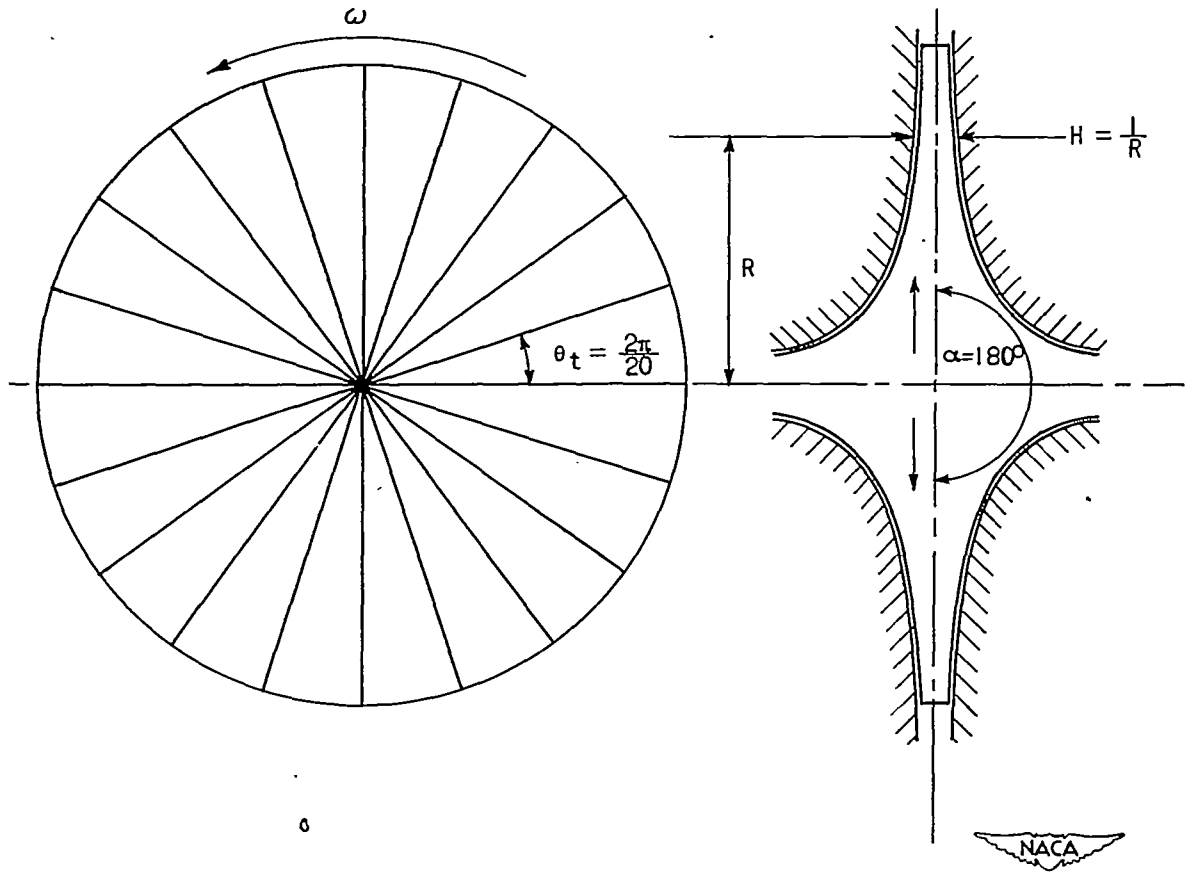


Figure 9. - Compressor design characteristics for numerical example.

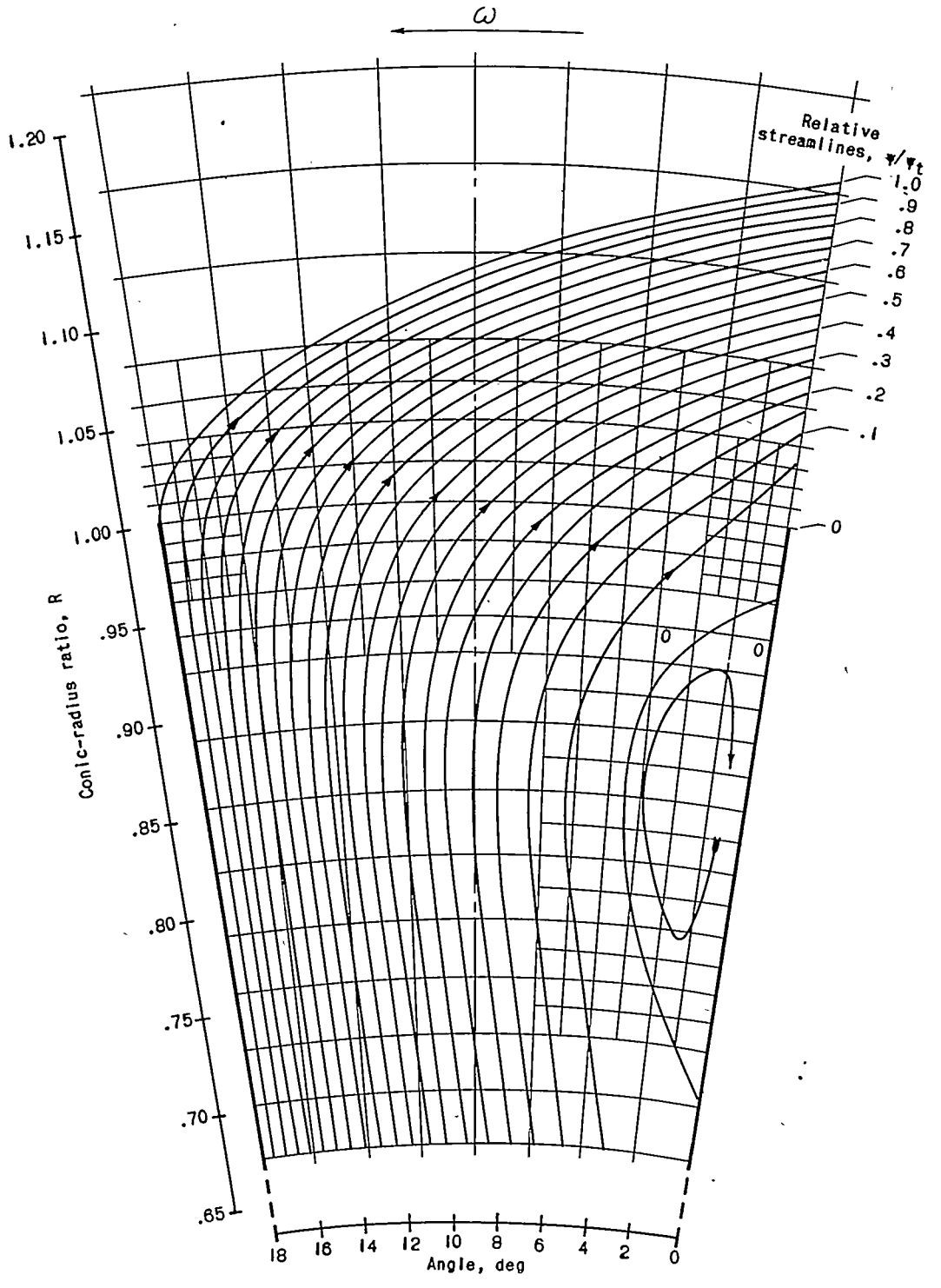


Figure 10. - Relative streamlines for compressible flow through centrifugal compressor. Streamline designation indicates percentage of flow through passage between streamline and right side of passage. Passage angle, 18 degrees; impeller tip Mach number $M_T$, 1.5; flow coefficient $\varphi$, 0.5; constant flow area (m, -1.0).

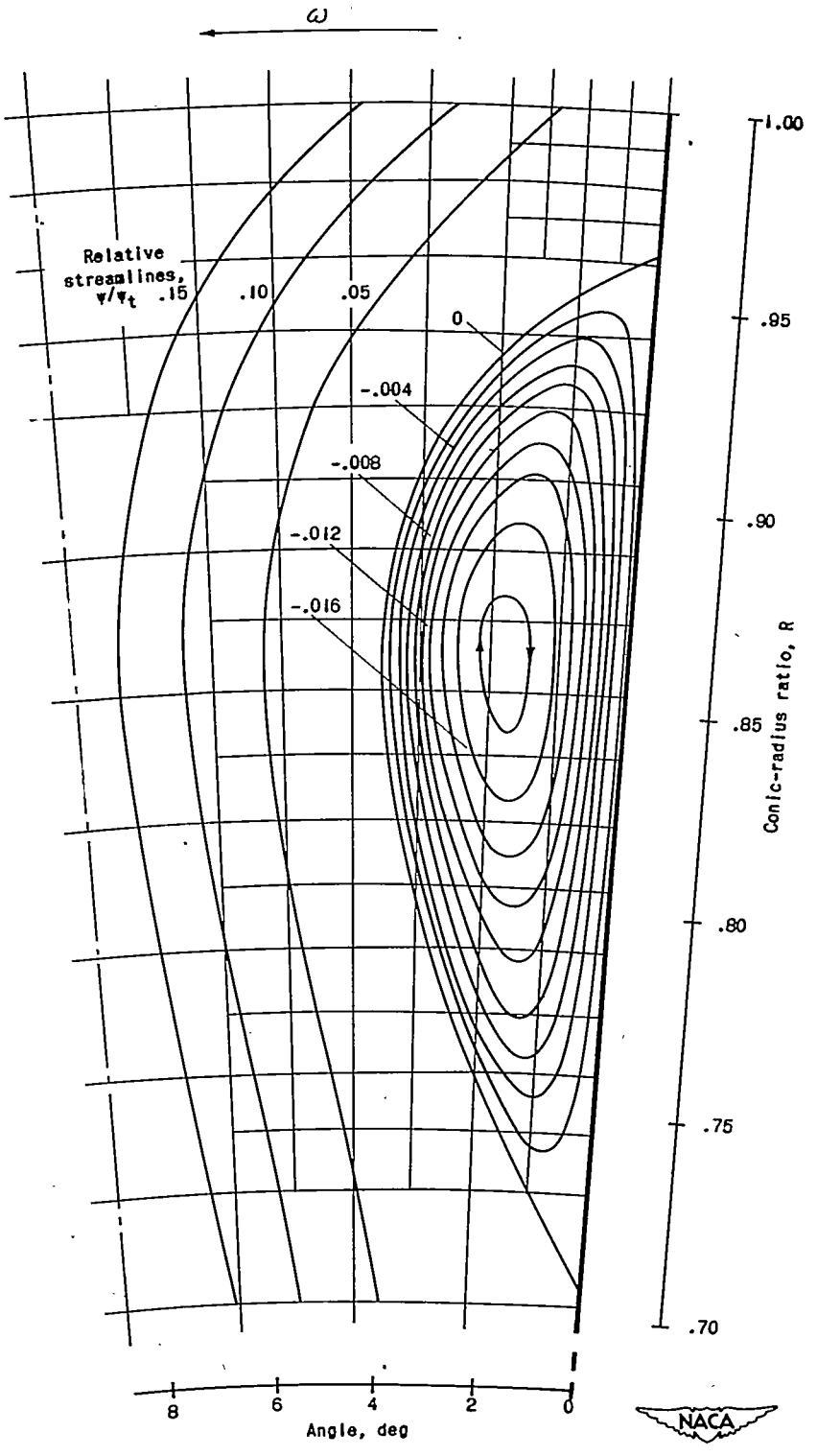


Figure 11. - Vortex on driving face of blade. Relative streamlines for every 0.2 percent of flow through impeller passage. Passage angle, 18 degrees; impeller tip Mach number $M_T$, 1.5; flow coefficient $\varphi$, 0.5; constant flow area (m, -1.0).

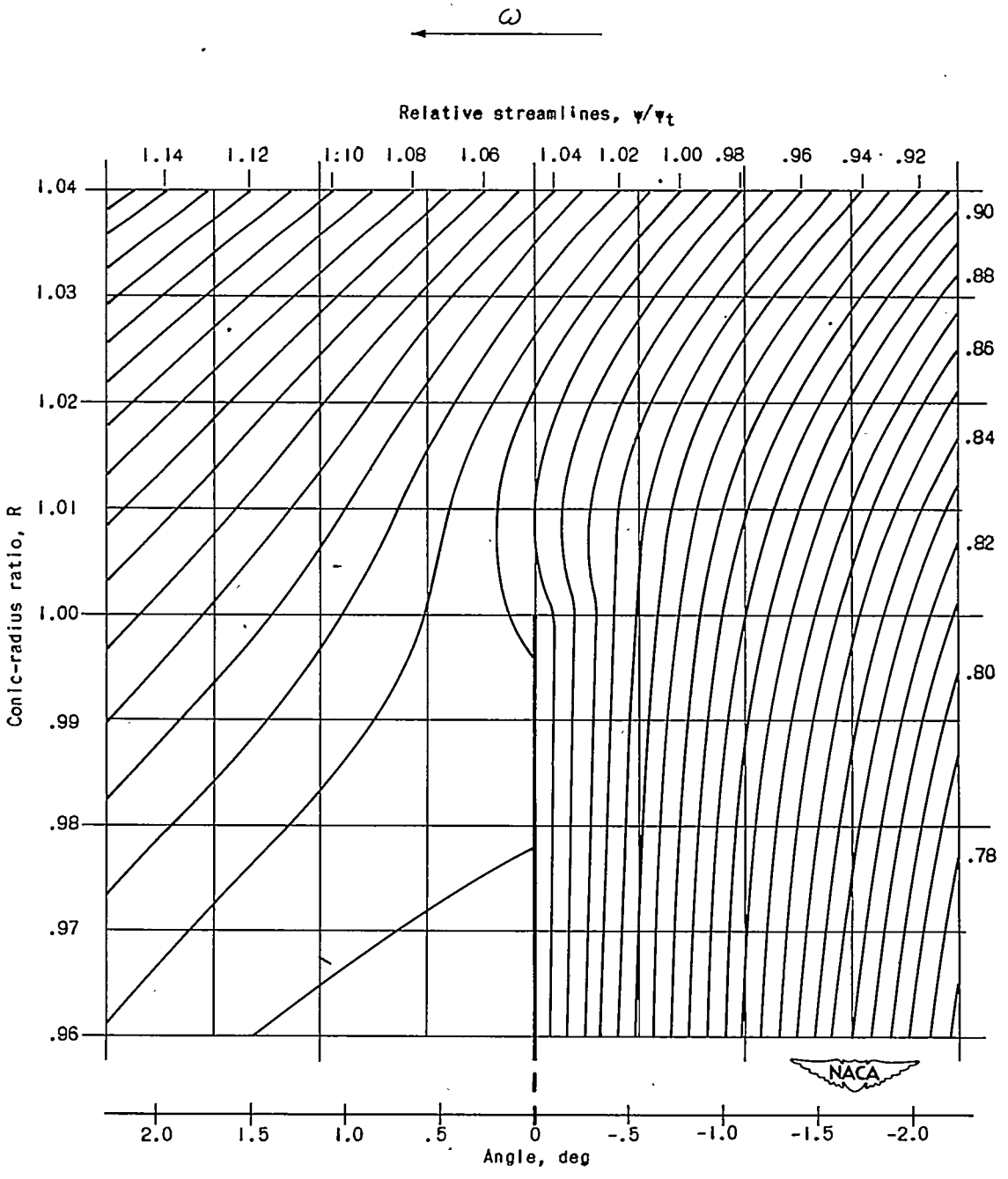


(a) Second attempt to satisfy Kutta condition of flow tangency at blade tip.

Figure 12. - Expanded view of relative streamlines in region of blade tip. Passage angle, 18 degrees; impeller tip Mach number $M_T$, 1.5; flow coefficient $\varphi$, 0.5; constant flow area (m, -1.0).

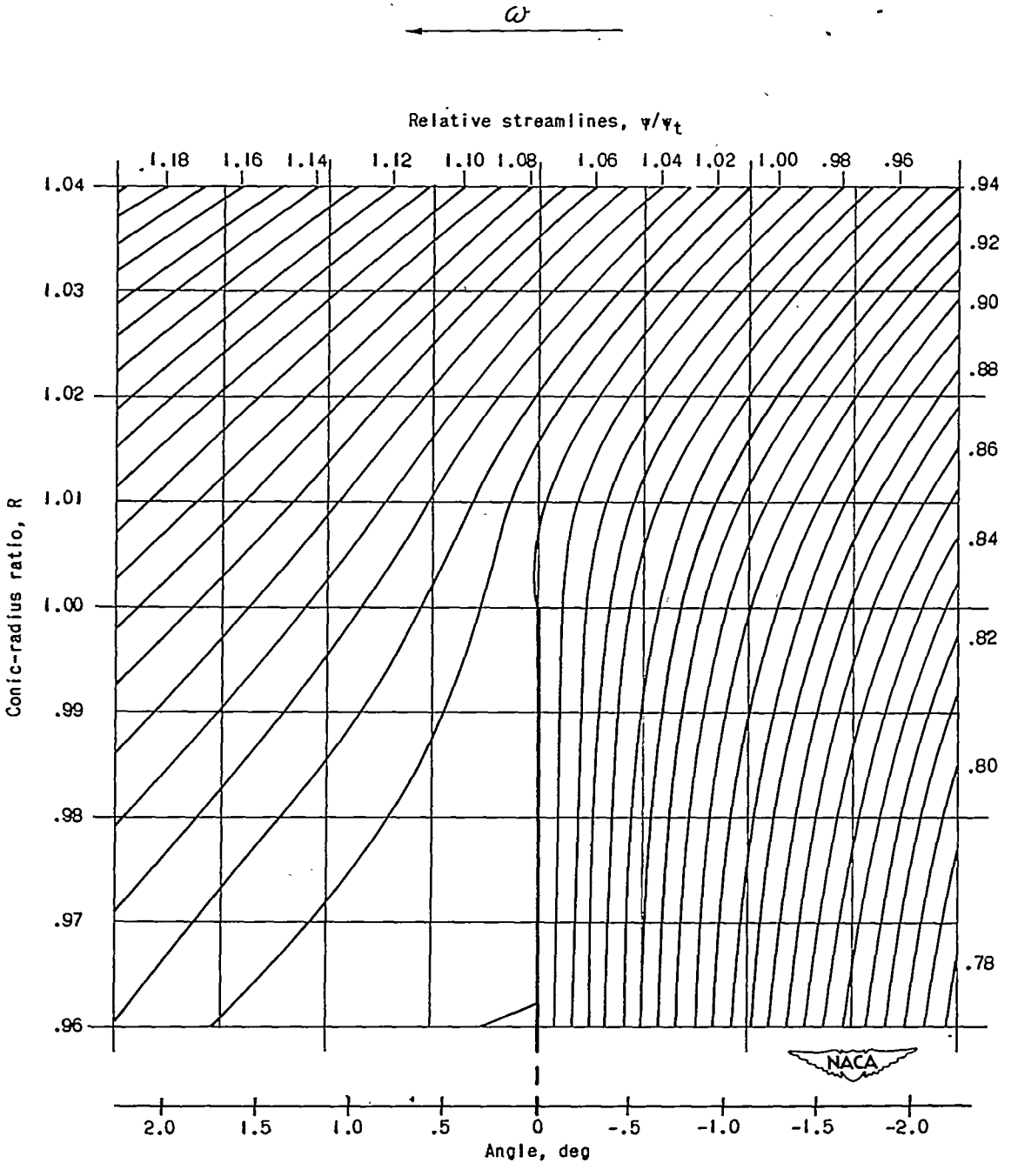


(b) Third attempt to satisfy Kutta condition of flow tangency at blade tip.

Figure 12. - Concluded. Expanded view of relative streamlines in region of blade tip. Passage angle, 18 degrees; impeller tip Mach number $M_T$, 1.5; flow coefficient $\varphi$, 0.5; constant flow area (m, -1.0).

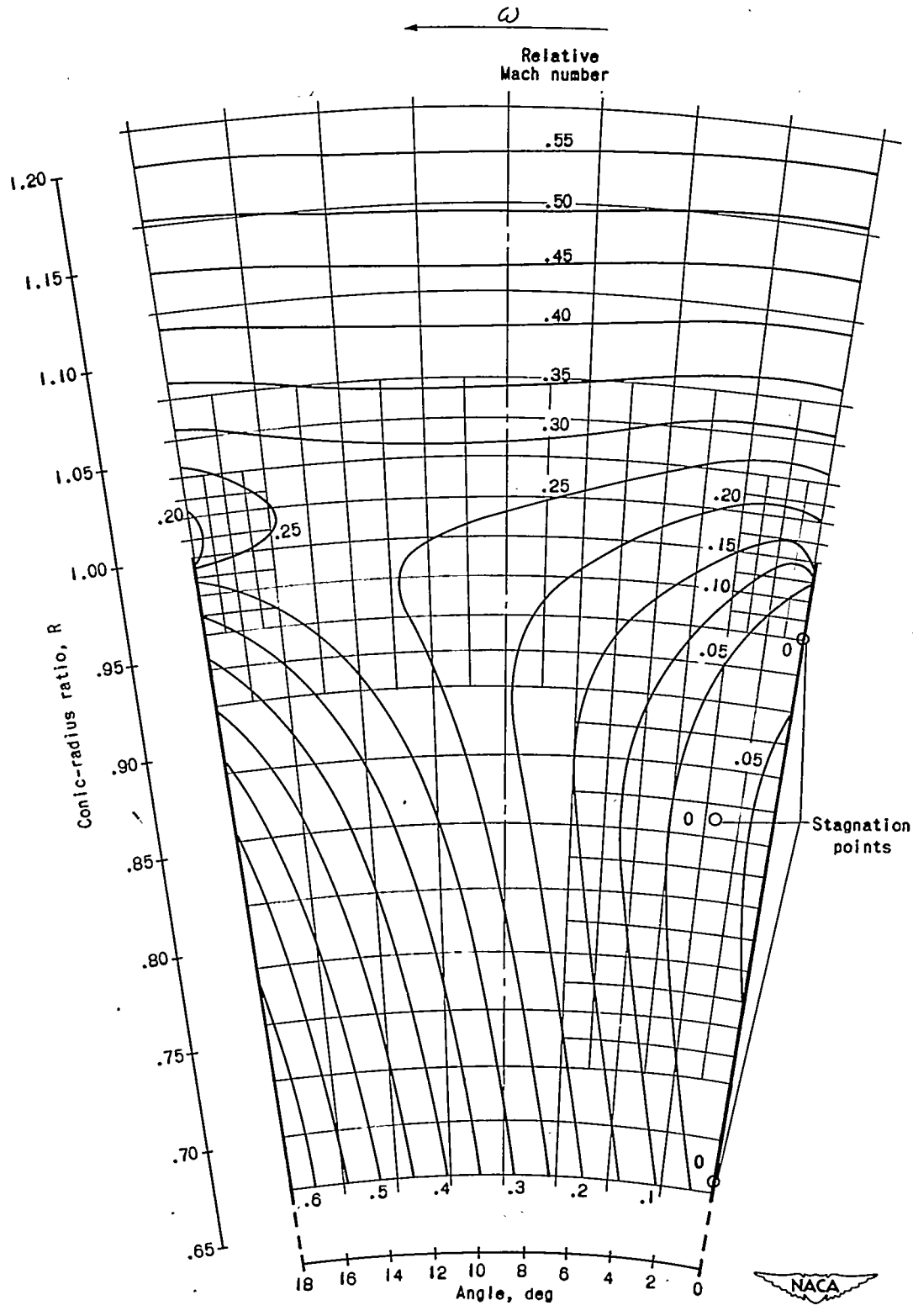


Figure 13. - Lines of constant Mach number relative to impeller. Passage angle, 18 degrees; impeller tip Mach number $M_T$, 1.5; flow coefficient $\varphi$, 0.5; constant flow area (m, -1.0).

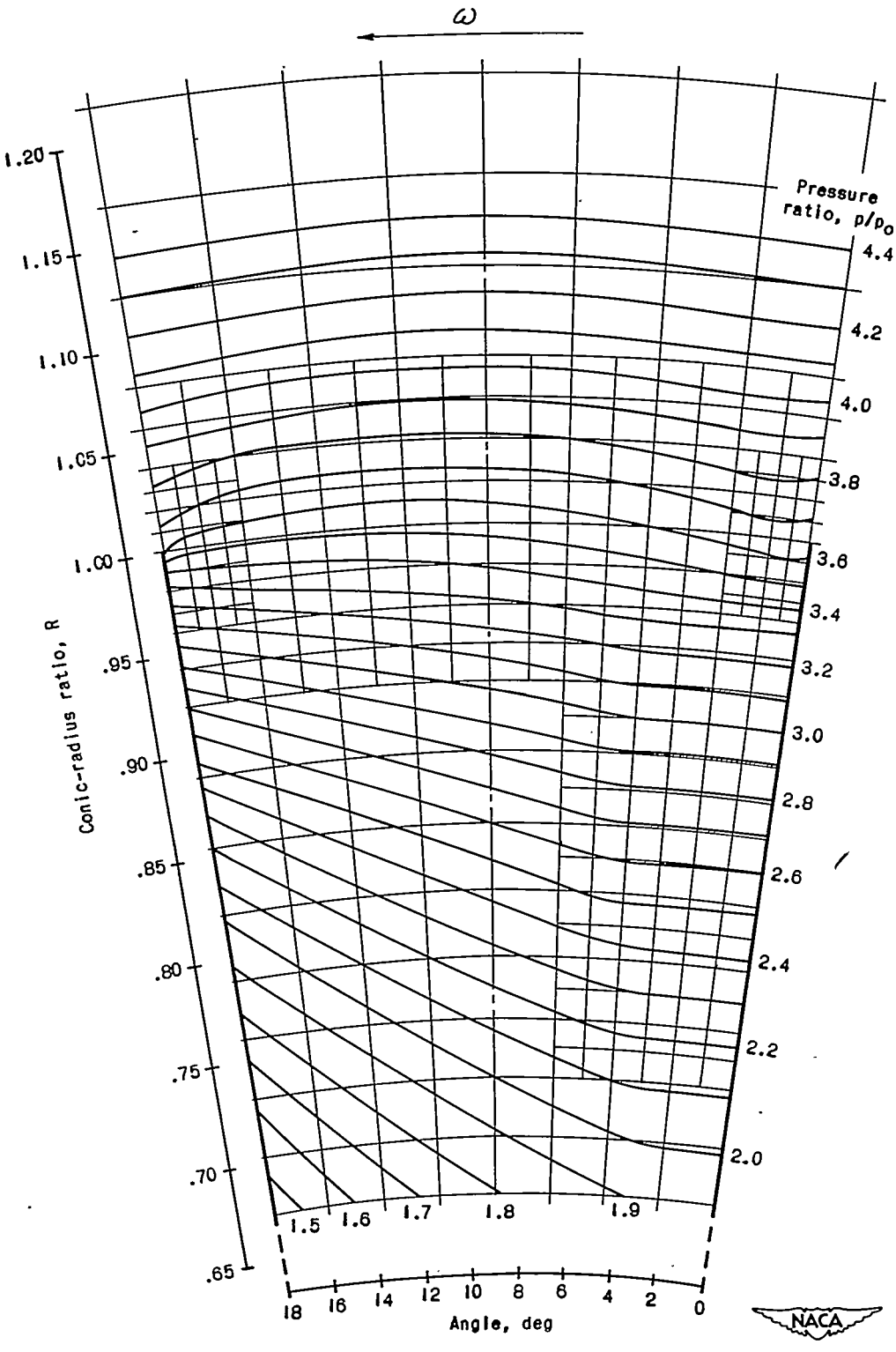


Figure 14. - Lines of constant pressure ratio. Passage angle, 18 degrees; impeller tip Mach number $M_T$, 1.5; flow coefficient $\varphi$, 0.5; constant flow area (m, -1.0).

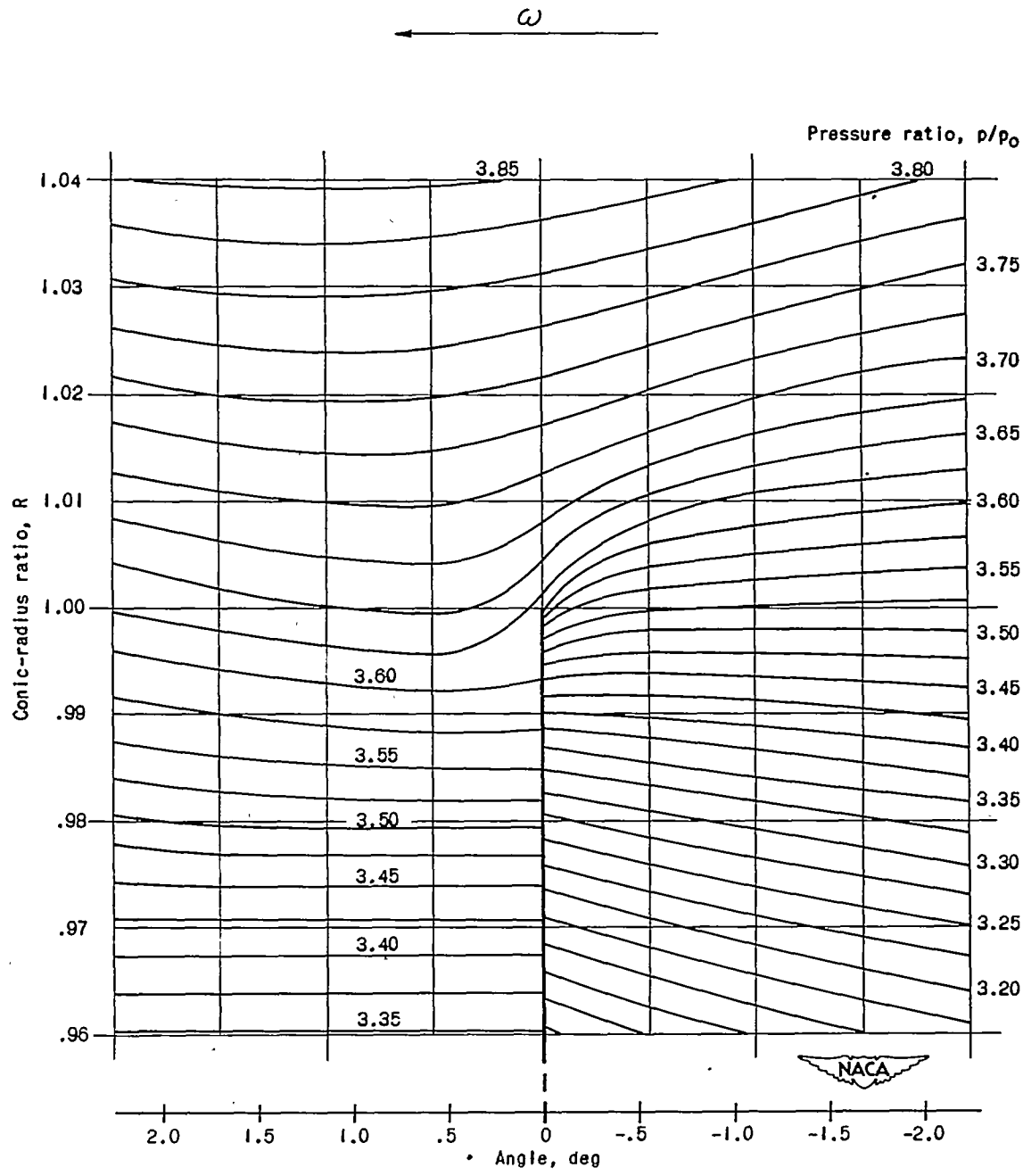


Figure 15. - Expanded view of pressure-ratio lines in vicinity of blade tip. Passage angle, 18 degrees; impeller tip Mach number $M_T$, 1.5; flow coefficient $\varphi$, 0.5; constant flow area (m, -1.0).

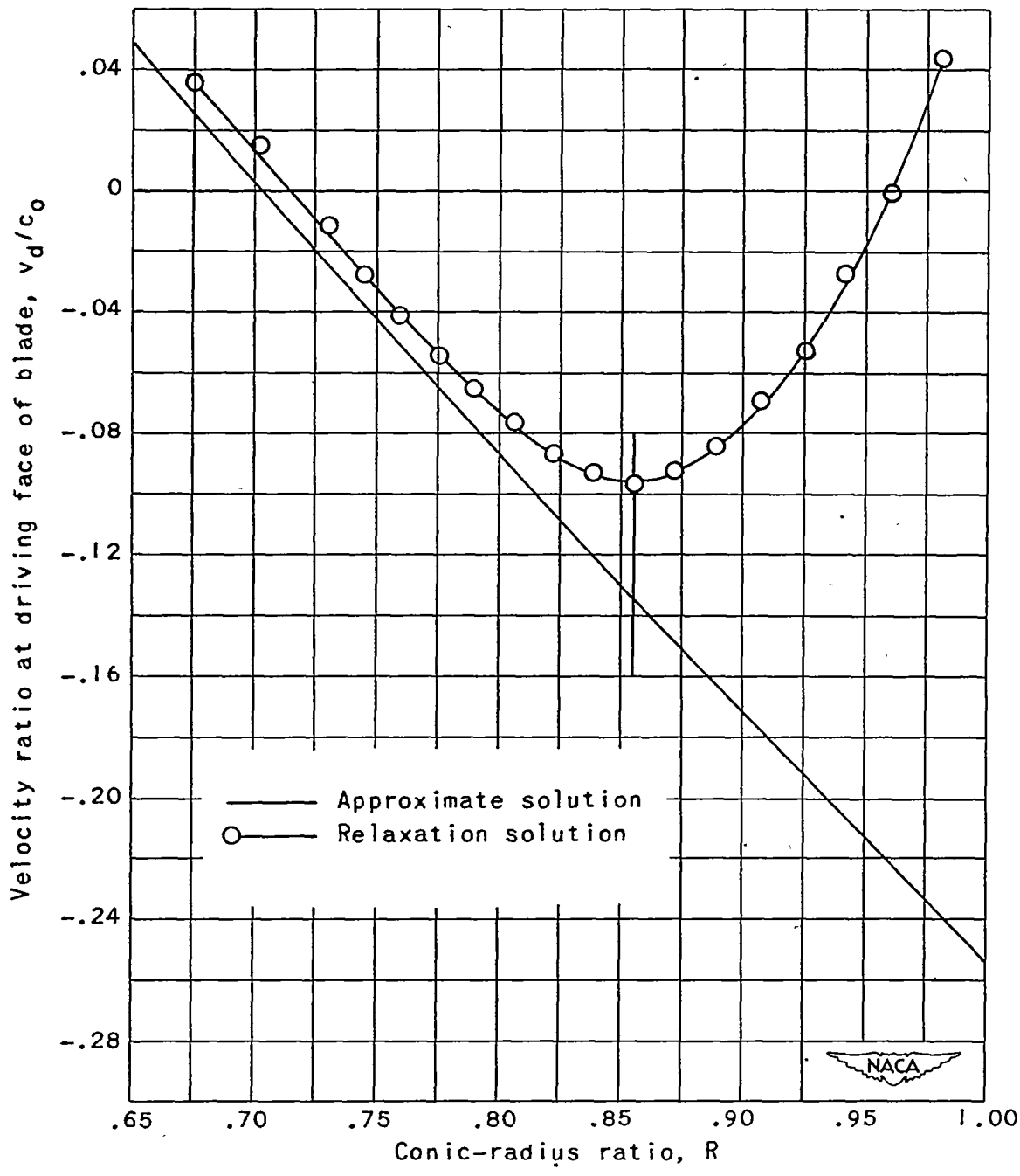


Figure 16. – Comparison of velocity ratio along driving face of blade for approximate and relaxation solutions.

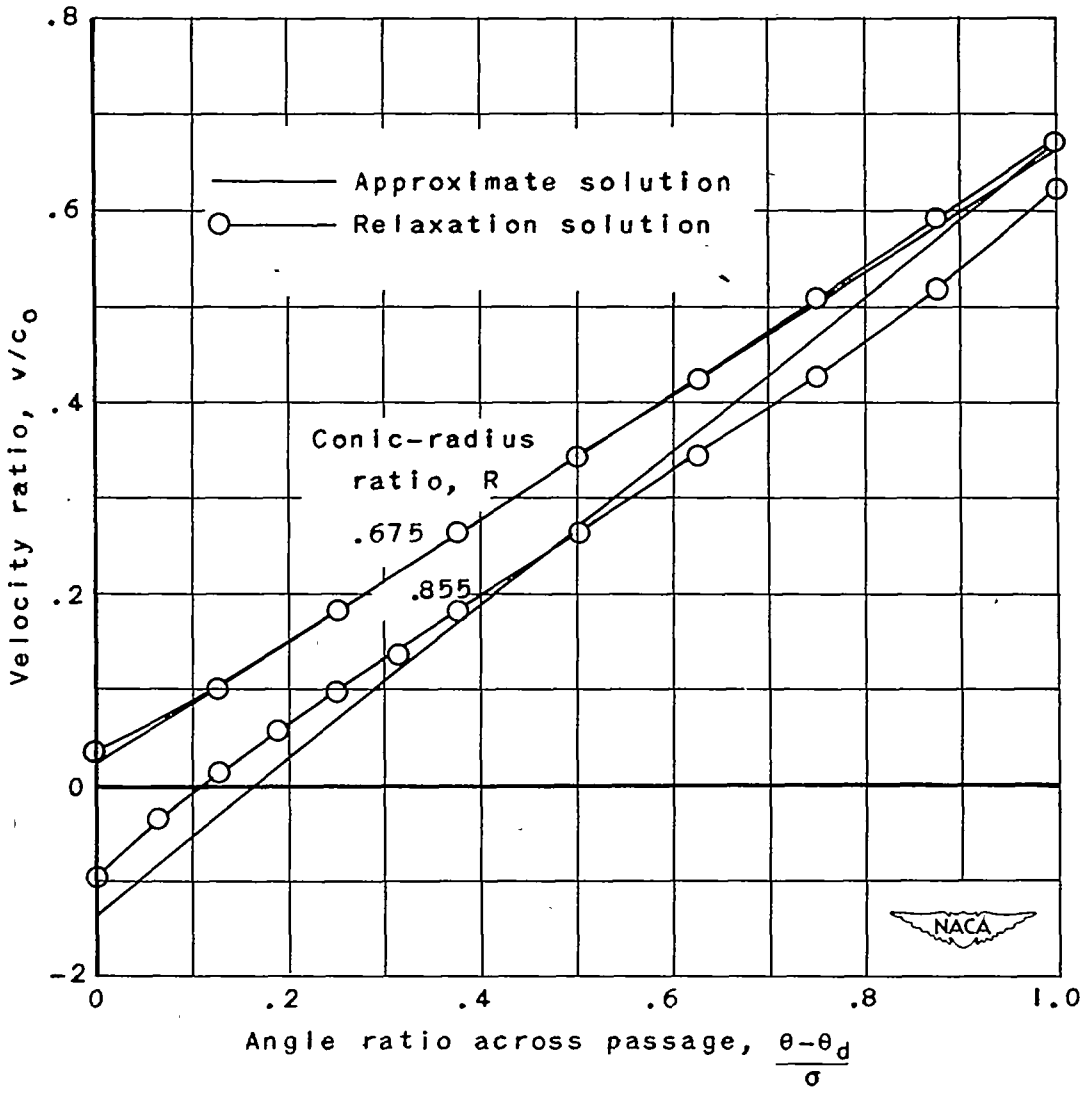


Figure 17. - Comparison of velocity distribution across passage for approximate and relaxation solutions.

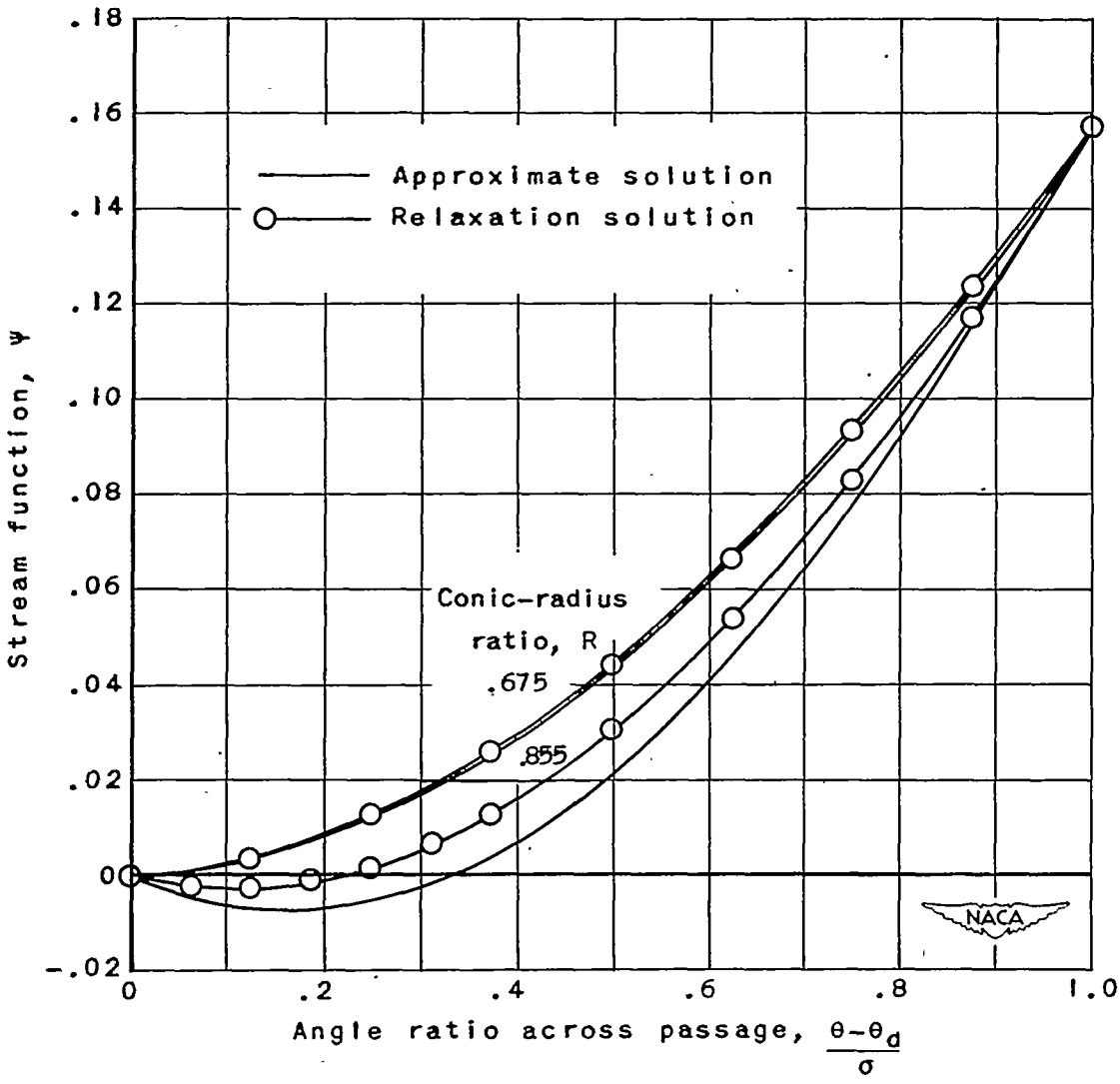


Figure 18. - Comparison of stream-function distribution across passage for approximate and relaxation solutions.

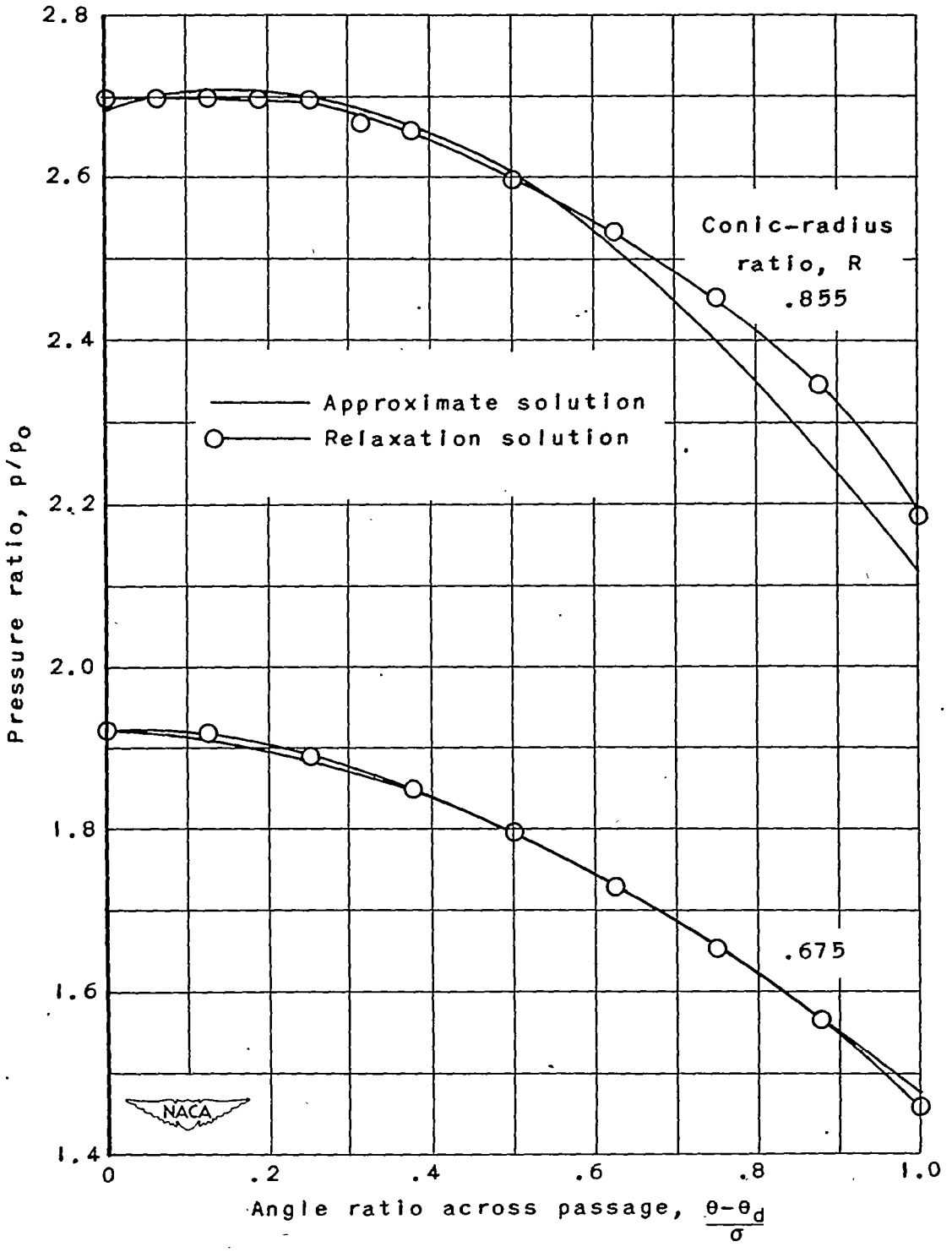


Figure 19. - Comparison of pressure-ratio distribution across passage for approximate and relaxation solutions.

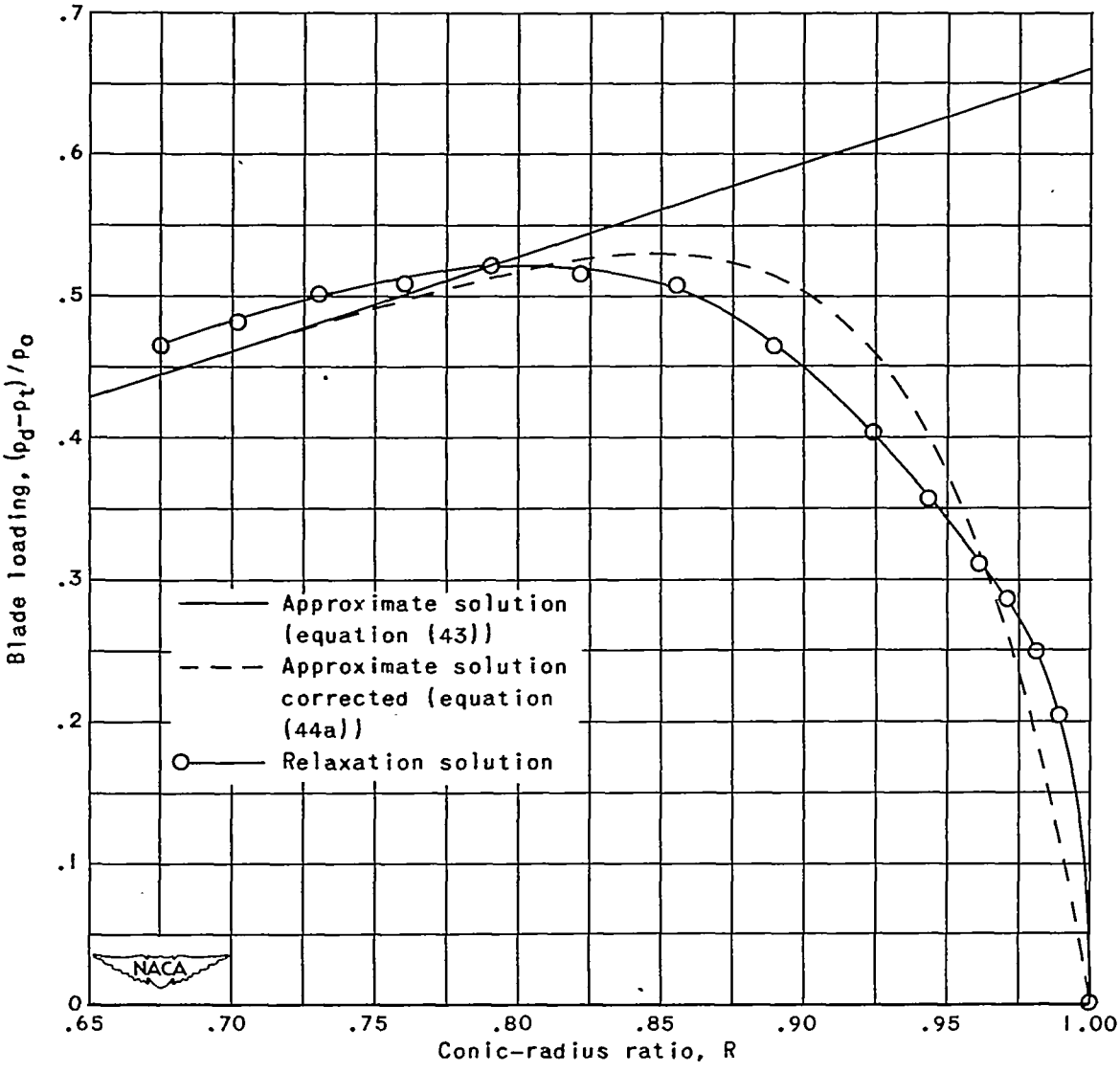


Figure 20. - Comparison of blade loading for approximate and relaxation solutions.

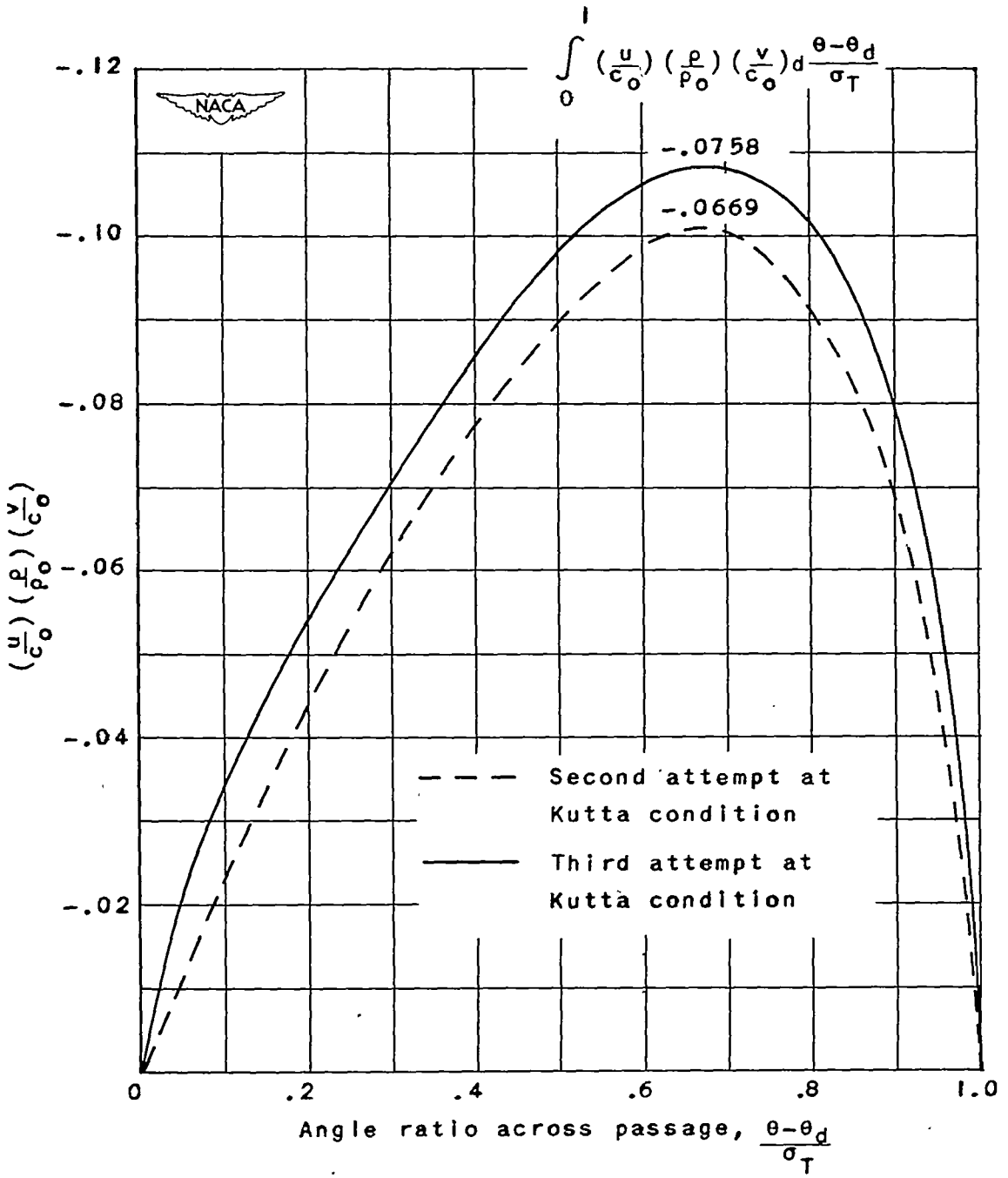


Figure 21. - Variation in integrand (for computing impeller slip) across passage at impeller tip. Second and third attempts to satisfy the Kutta condition.